



Published in final edited form as:

Nat Metab. 2020 May ; 2(5): 397–412. doi:10.1038/s42255-020-0205-x.

Human thermogenic adipocyte regulation by the long noncoding RNA LINC00473

Khanh-Van Tran^{1,2,8}, Erin Louise Brown^{5,8}, Tiffany DeSouza¹, Naja Zenius Jespersen³, Cecilie Nandrup-Bus³, Qin Yang¹, Zinger Yang¹, Anand Desai¹, So Yun Min¹, Raziel Rojas-Rodriguez¹, Morten Lundh⁵, Amir Feizi⁷, Hanni Willenbrock⁴, Therese Juhlin Larsen³, Mai Charlotte Krogh Severinsen³, Kimberly Malka⁶, Anthony M. Mozzicato⁵, Atul S. Deshmukh⁵, Brice Emanuelli⁵, Bente Klarlund Pedersen³, Timothy Fitzgibbons^{1,2}, Camilla Scheele^{3,5}, Silvia Corvera^{1,9}, Søren Nielsen^{3,9}

¹Program in Molecular Medicine, University of Massachusetts Medical School, Worcester, MA 01655, USA

²Department of Medicine, Division of Cardiovascular Medicine, University of Massachusetts Medical School, Worcester, MA 01655, USA

³The Centre of Inflammation and Metabolism and the Centre for Physical Activity Research, Rigshospitalet, University of Copenhagen, Copenhagen, Denmark

⁴Novo Nordisk A/S, Discovery Biology & Technology, Bioinformatics, Maaloev, Denmark

⁵Novo Nordisk Foundation Center for Basic Metabolic Research, Faculty of Health and Medical Science, University of Copenhagen, Copenhagen, Denmark

⁶Department of Surgery, Division of Vascular and Endovascular Surgery, University of Massachusetts Medical School, Worcester, MA 01655, USA

⁷Novo Nordisk Research Centre Oxford, University of Oxford, United Kingdom

⁸Co-first authors

⁹Co-senior authors

Abstract

Human thermogenic adipose tissue mitigates metabolic disease, raising much interest in understanding its development and function. Here, we show that human thermogenic adipocytes specifically express a primate-specific long non-coding RNA, *LINC00473* which is highly correlated with UCP1 expression and decreased in obesity and type-2 diabetes. *LINC00473* is detected in progenitor cells, and increases upon differentiation and in response to cAMP. In

Users may view, print, copy, and download text and data-mine the content in such documents, for the purposes of academic research, subject always to the full Conditions of use:http://www.nature.com/authors/editorial_policies/license.html#terms

Corresponding author: Silvia.Corvera@umassmed.edu.

Author Contributions

S.C. and S.N. supervised this work. K.V.T., E.L.B., T.D., C.N.B., S.Y.M., M.L., T.J.L., B.E., B.K.P., T.F., C.S., S.N., S.C.: hypothesis generation, conceptual design, data analysis, and manuscript preparation. K.V.T., E.L.B., T.D., N.Z.J., C.N.B., Q.Y., Z.Y., A.D., S.Y.M., R.R.R., A.F., H.W., M.C.K.S., K.M., A.M.M., A.S.D., S.C., S.N.: conducting experiments and data analysis.

Competing Interests Statement

The authors declare no competing interests.

contrast to other known adipocyte lincRNAs, LINC00473 shuttles out of the nucleus, colocalizes and can be crosslinked to mitochondrial and lipid droplet proteins. Up- or down- regulation of *LINC00473* results in reciprocal alterations in lipolysis, respiration and transcription of genes associated with mitochondrial oxidative metabolism. Depletion of PLIN1 results in impaired cAMP-responsive *LINC00473* expression and lipolysis, indicating bidirectional interactions between PLIN1, LINC00473 and mitochondrial oxidative functions. Thus, we suggest that *LINC00473* is a key regulator of human thermogenic adipocyte function, and reveals a role for a lincRNA in inter-organelle communication and human energy metabolism.

Keywords

brown; beige; brite; norepinephrine; forskolin; adipocyte; mitochondria; respiration; non-coding RNA; fat; lipid droplet; lipolysis; PLIN1

Adipose tissue is central to the control of whole-body energy homeostasis, playing pivotal roles such as energy storage and release, endocrine control of fuel homeostasis, and thermogenesis¹⁻⁵. Thermogenic adipose tissue, such as classical interscapular brown or inguinal brite/beige, is defined by the presence of adipocytes expressing the mitochondrial uncoupling protein UCP1. In the past decade, it has been shown that the abundance of active thermogenic adipose tissue in humans is strongly associated with body mass index, increased energy expenditure and improved glucose homeostasis^{6,7}. These findings have prompted increasing interest in understanding the mechanisms that lead to the development and maintenance of thermogenic adipose tissue in humans⁸⁻¹⁰.

In mice, genetic lineage tracing has been leveraged for identification of adipose tissue development¹¹⁻¹³. Unexpectedly, these studies have shown that a single adipose depot can contain adipocytes from different lineages¹¹. In addition to developmental lineage, anatomical localization influences adipose tissue development as adipocyte progenitors transplanted into different regions of mice give rise to functionally different adipose tissues¹⁴. Human thermogenic adipose tissue depots are comprised of mixtures of white and thermogenic adipocytes. Thus, to understand the development of human thermogenic adipose tissue, it is necessary to uncover the mechanisms by which individual adipocytes develop and maintain their phenotypes within specific human adipose depots.

Recent transcriptomic analyses have revealed thousands of non-coding RNAs which can potentially regulate development and differentiation at multiple levels, including chromatin modification, transcription and post transcriptional processing¹⁵⁻¹⁷. In mice, long non-coding RNAs (lncRNAs), which are located either as independent units between two coding genes or intronic located, have been shown to play a role in adipocyte development. A nuclear lncRNA, Blinc1, is implicated in the development of thermogenic adipocytes through a ribonucleoprotein complex containing the transcription factor EBF2¹⁸. Another lncRNA, lncBATE10, can prevent repression of Ppargc1a mRNA and sustain the thermogenic phenotype^{19,20}. Thus, lncRNAs could be central players in integrating anatomical and lineage factors to produce functionally distinct adipocytes residing in different depots.

While lineage tracing cannot be performed in humans, relevant information can be derived from multipotent mesenchymal adipocyte progenitors present within adipose tissue. In previous studies, we observed that human adipocyte progenitor cells associated with the adipose tissue microvasculature differentiate into diverse functional subtypes^{10,21}, and that the human thermogenic fat differentiation program is cell autonomous and depot-related⁸. In this paper, we leveraged these findings to investigate the gene expression signatures of progenitors and differentiated adipocytes from different human adipose tissue depots to define genes associated with the development of thermogenic adipocytes. We find that the primate-specific lncRNA, *LINC00473*, appears early in the development of human thermogenic adipocytes, increases with differentiation and is strongly induced by activation of thermogenic adipocytes.

While previously identified long non-coding RNAs associated with adipocyte development act through nuclear transcriptional regulation, *LINC00473* operates through a role in metabolism, being shuttled to the cytoplasm where it interacts with mitochondrial and lipid droplet targets, modulating mitochondrial responsiveness and lipolysis. These findings reveal a key role for a long non-coding RNA to affect fundamental aspects of thermogenic adipocyte physiology necessary for the development and function of human thermogenic adipose tissue.

Results

Identification of *LINC00473* as a specific marker of human thermogenic adipocytes

To elucidate the mechanisms involved in the generation of thermogenic adipocytes in humans, we first searched for major gene expression differences between adipocytes generated from mostly non-thermogenic and thermogenic adipose tissue depots. Biopsies from abdominal subcutaneous (AbdSQ) and from supraclavicular (SCLav) adipose tissue of non-diabetic subjects were obtained (Supplementary Table 1, subject characteristics). Stromovascular cells extracted by collagenase digestion were differentiated as depicted in Figure 1a and b. Differentiated adipocytes were stimulated for 4h with norepinephrine (NE) prior to RNASeq. SCLav and AbdSQ derived adipocytes identified 29,907 annotated genes, which segregated in the first principal component into two main groups corresponding to the two depots of origin (Figure 1c). Unsupervised hierarchical clustering of the 1000 most varied genes also produced two main clusters (Figure 1d), with further segregation within each cluster. Segregation within the AbdSQ cluster was determined by individual subjects, while segregation within the SCLav cluster was determined by NE stimulation, underscoring the dominance of the NE-induced gene expression program in all subjects.

We searched for genes that responded to NE in cells from both AbdSQ and SCLav from all subjects. This group of genes contained the long non-coding RNA, *LINC00473* (Figure 1d), which was among the most strongly induced of the 313 genes significantly regulated by NE (Figure 1e,f and Supplementary Table 2). Levels of genes previously reported as selective markers for thermogenic and white adipose tissue (*HOXC8*, *HOXC9*, *TBX1*) or as activated by adrenergic stimulation (*UCP1* and *DIO2*) were consistent with prior work of others (Figure 1f), validating our current analysis. To address whether *LINC00473* levels vary with human physiological states, we analyzed its expression in supraclavicular adipose tissue

from a large cohort of humans with differing BMI and diabetes status. *LINC00473* levels were higher in supraclavicular than in subject-matched abdominal subcutaneous adipose tissue (Figure 1g) and were strongly correlated with *UCPI* levels (Figure 1h). *LINC00473* levels were decreased in supraclavicular samples derived from overweight, obese and type 2 diabetic subjects (Figure 1i) concordant with decreased levels of thermogenic adipose tissue abundance reported in similar populations²².

To further define the relationship between *LINC00473* and thermogenic adipocyte development, we studied mesenchymal progenitor cells from human adipose tissue depots, obtained through culture of explants under pro-angiogenic conditions¹⁰. Mesenchymal progenitors from the neck (NeckSQ) and from carotid perivascular adipose tissue (Carotid) grew robustly (Figure 2a), and readily differentiated and responded to Forskolin (Fsk), as seen by the decrease in lipid droplet size after 6h of exposure (Figure 2b, middle and right panels, arrows). Adipocyte-specific genes *PLIN1*, *ADIPOQ* and *FABP4* were similarly induced upon differentiation of progenitors from both depots (Figure 2c–e). In contrast, basal *UCPI* expression was only detected in adipocytes differentiated from NeckSQ (Figure 2f), consistent with a more pronounced thermogenic pre-programming in these cells compared to those from other depots. Nevertheless, adipocytes differentiated from progenitor cells from all depots responded to Fsk with strong increases in *UCPI* (Figure 2g), indicating that all human depots can potentially recruit thermogenic adipocytes, as seen *in vivo* during extreme physiological conditions such as extensive burn stress^{23,24}.

To identify genes associated with generation of thermogenic adipocytes in different human depots, we conducted a multi-group differential expression analysis comparing adipocytes differentiated from AbdSQ, NeckSQ and Carotid mesenchymal progenitors, with or without Fsk stimulation. Patterning gene transcripts (*HOX*, *TBX*, *MSX*, *LHX* gene families) from adipocytes differentiated from AbdSQ, NeckSQ and Carotid progenitors segregated in two clusters corresponding to central (AbdSQ) and cranial (NeckSQ and Carotid) depots (Figure 2h), indicating that even after proliferation and differentiation *in vitro*, adipocytes maintain gene expression signatures associated with their depot of origin. Importantly, unsupervised hierarchical clustering of genes differentially expressed among all conditions (385 genes, Supplementary Table 3) resulted in 6 clusters, indicating that the Fsk response depends on the depot of origin, possibly due to the different abundance of thermogenic adipocytes in each depot (Figure 2i). To determine which genes define depot-specific responsiveness to Fsk, we calculated the median absolute deviation of transcripts in this set. The topmost gene transcript in this analysis corresponded to *LINC00473* (Supplementary Table 3), pointing to this gene as the most closely associated with Fsk responsiveness of human adipose tissue depots. Interestingly, *LINC00473* upregulation in response to NE seems cell type specific, as among a cell panel of adrenergically responsive cell types, only thermogenic adipocytes and smooth muscle cells upregulated *LINC00473*, whereas cardiac myocytes and skeletal myocytes did not respond (Supplementary Figure 1).

We then asked at what stage of thermogenic adipocyte development *LINC00473* is expressed. We found that *LINC00473* levels were higher in progenitors derived from the NeckSQ or Carotid compared to AbdSQ depots (Figure 2j) and increased to a significantly higher level in adipocytes from these depots (Figure 2k). As expected, *LINC00473* was

strongly induced by Fsk, more so in adipocytes from NeckSQ and Carotid depots compared to those from AbdSQ (Figure 2l). Interestingly, *LINC00473* expression in progenitor cells was directly correlated with Fsk-stimulated *UCP1* expression in subsequently differentiated adipocytes (Figure 2m), suggesting that *LINC00473* expression in progenitor cells defines subsequent adipocyte thermogenic capacity.

LINC00473 localizes to the mitochondrial/ lipid droplet interphase

To explore potential roles of *LINC00473* in thermogenic adipocyte development and function, we first investigated its subcellular localization. Time course analysis indicated that both NE (Figure 3a) and Fsk (Figure 3b) stimulate *LINC00473* expression acutely, with a peak after approximately 6h of stimulation similar to the peak induction of *UCP1* (3b). In situ hybridization revealed that during the first 3h after Fsk addition, *LINC00473* appeared within well-defined nuclear loci reminiscent of nucleoli, but subsequently the majority of *LINC00473* shuttled into the cytoplasmic space (Figure 3c). This movement was specific to *LINC00473*, as the nuclear lncRNA *MALAT1* remained in the nucleus under both basal and Fsk stimulated conditions (Figure 3d).

To explore potential roles of *LINC00473* in the cytoplasm, we used mass spectrometry-based proteomics to identify interacting proteins. Cells stimulated with Fsk for 6h were subjected to cellular fractionation to remove the nuclear fraction. The supernatant was then crosslinked by exposure to UV light, and biotinylated short oligonucleotide probes tiling the length of *LINC00473* were used for hybridization. Capture of hybridized complexes with streptavidin-coupled magnetic beads resulted in recovery of approximately 10% of total *LINC00473* (Figure 3e). The top proteins associated with the complex corresponded to FABP5, PLIN1 and ACOT1/2 (Figure 3f), which are involved in lipid transport and metabolism. Pathway analysis of detected peptides revealed enrichment in mitochondrial compartments in addition to lipid droplet proteins (Figure 3g). To verify the findings from the proteomics analysis we performed immunoprecipitation of crosslinked extracts with antibodies to PLIN1 followed by detection of *LINC00473* by RT-PCR. Specific signal was detected only in immunoprecipitants from Fsk-stimulated adipocytes, and not in extracts from non-stimulated cells or in control IgG precipitated extracts (Figure 3h,i). Lastly, we used RPISeq, a computational approach to predict RNA-protein interactions based on amino acid and nucleotide sequences²⁵, and found that an interaction between PLIN1 and *LINC00473* is very likely (SVM=0.9, RF=0.85).

To further validate the finding of interactions between *LINC00473*, PLIN1 and mitochondrial proteins, we conducted subcellular fractionation to examine whether *LINC00473* co-purifies with these organelles. We find that the mitochondrial DNA encoded ATP Synthase Membrane Subunit 6 transcript (*ATP6*) and *LINC00473* co-sediment away from nuclear *MALAT1* upon differential centrifugation (Figure 4a). Moreover, both *LINC00473* and *ATP6* are enriched in the floating fraction containing the majority of lipid droplets following cellular fractionation (Figure 4b). To more precisely define the localization of *LINC00473* relative to mitochondria and lipid droplets we used super resolution confocal imaging with antibodies to mitochondrial Hsp70 and PLIN1. In non-stimulated cells, PLIN1 smoothly decorated the outline of large lipid droplets (Figure 4c,

0h), but in response to Fsk, PLIN1 became fractured, with some lipid droplets only retaining remnants of the PLIN1 signal (Figure 4c, 6h). Under these conditions *LINC00473* formed higher-order structures that co-localized both with Hsp70 and PLIN1 (Figure 4c, right panel magnification). Quantification of the extent of co-localization revealed 20% and 40% colocalization of *LINC00473* particles with PLIN1 and Hsp70, respectively, and 20% colocalization with areas where PLIN1 and HSP70 co-localize (Figure 4d).

To further probe the physical and functional interactions between *LINC00473*, PLIN1 and mitochondria we examined the consequences of PLIN1 knockdown. Cells were transfected at day 5 of differentiation using 3 separate siRNA oligonucleotides, and *PLIN1* mRNA levels were assessed 48h later. All three oligonucleotides resulted in over 80% decrease in *PLIN1* mRNA compared to cells transfected with a scrambled oligonucleotide, and this level of knockdown was maintained after 6 h of Fsk stimulation (Figure 4e). To assess the functional consequence of PLIN1 knockdown, we measured the amount of glycerol accumulated in the medium during the 48h following transfection. Knockdown of PLIN1 resulted in significantly increased levels of glycerol, consistent with increased basal lipolysis (Figure 4f). Interestingly, knockdown of PLIN1 resulted in greatly decreased *LINC00473* levels following Fsk stimulation (Figure 4g), which was accompanied by significant suppression of Fsk-stimulated lipolysis (Figure 4h). After PLIN1 knockdown, the total area occupied by *LINC00473* signal was reduced (Figure 4i and 4j, Total area) due to a decrease in both the number of *LINC00473* particles (Figure 4j, Number of particles) and their average size (Figure 4j, Average size). PLIN1 knockdown did not affect the total mitochondrial density, as assessed by total area of Hsp70 in binarized images (Figure 4k, Total area) but did result in a significant decrease in number of particles (Figure 4k, Number of particles), with a corresponding increase in size (Figure 4k, Average size), suggesting an alteration in mitochondrial fission/fusion activity. The number of *LINC00473* particles co-localized with mitochondria decreased in response to PLIN1 knockdown, and the size of the *LINC00473* particles colocalizing with mitochondria tended to be larger (Figure 4l). These results support a physical and functional interaction between PLIN1, *LINC00473* and mitochondria, and suggest that this interaction may directly or indirectly impact mitochondrial fusion/fission activity.

LINC00473 modulates lipolysis and mitochondrial respiration

To determine whether *LINC00473* may regulate lipolysis and mitochondrial function directly, we explored the effects of depletion and overexpression of *LINC00473* on both lipolysis and oxygen consumption. *LINC00473* levels in response to NE were significantly decreased in cells transfected with a pool of oligonucleotides targeted to *LINC00473* (Figure 5a). *LINC00473* knockdown resulted in decreased levels of basal and FCCP-induced respiration after addition of NE, suggesting an overall decrease in mitochondrial capacity (Figure 5 b,c). To explore the effects of increasing *LINC00473*, we used CRISPR-SAM to stimulate its expression through its own endogenous promoter. This resulted in up-regulation of basal *LINC00473* expression that could be detected without stimulation, and a further >100-fold greater induction after stimulation by Fsk compared to those seen in empty-vector control cells (Figure 5d). The expression level of all splice variants of *LINC00473* that share the same promoter were increased (Figure 5e), but no increase was seen in the expression

levels of potential off targets within the same locus or with promoter region sequences similar to the sgRNA (Gd6) targeting the *LINC00473* promoter (Supplementary Table 4 and Supplementary Figure 2). CRISPR-SAM adipocytes overexpressing *LINC00473* (Gd6) displayed a higher respiration in response to Fsk, and increased degree of uncoupling (Figure 5f,g). To determine whether *LINC00473*-responsive changes in mitochondrial respiration were associated with changes in lipolysis, we measured free fatty acid release. Cells overexpressing *LINC00473* displayed a significantly higher lipolytic rate in response to Fsk, consistent with higher respiration (Figure 5h). In contrast, cells in which *LINC00473* expression was blunted using siRNA targeting the most abundant *LINC00473* transcript displayed decreased lipolytic rate compared to controls (Figure 5i). These functional effects of *LINC00473* overexpression or silencing were not attributable to significant changes in mitochondrial mass, as assessed by measurement of mitochondrial DNA levels in the conditions tested (Figure 5j).

To more fully understand the functional consequences of *LINC00473*-mediated modulation of mitochondrial respiration and lipolysis, we analyzed the transcriptome of cells overexpressing *LINC00473*, and that of cells in which *LINC00473* expression was blunted. In response to *LINC00473* overexpression, 314 transcripts were significantly increased and 262 decreased (Figure 6a and Supplementary Table 5). Pathways enriched in genes up-regulated in response to *LINC00473* overexpression included mitochondrial metabolic pathways, particularly lipid oxidation (Figure 6b); pathways enriched in genes down-regulated in response to *LINC00473* overexpression included interferon and cytokine signaling, and extracellular matrix organization (Figure 6c). In response to *LINC00473* depletion, 424 genes were up-regulated and 508 were down-regulated (Figure 6d and Supplementary Table 6). Pathways enriched in genes that were down-regulated in response to *LINC00473* depletion were similar to those enriched by genes up-regulated by *LINC00473* overexpression and corresponded to mitochondrial metabolic pathways (Figure 6e). Similarly, pathways enriched in genes that were up-regulated in response to *LINC00473* depletion were similar to those enriched by genes down-regulated by *LINC00473* overexpression and included cytokine signaling and extracellular matrix organization. The reciprocal effects of overexpression and depletion of *LINC00473* were further evidenced by the finding of 120 genes that were up-regulated by *LINC00473* overexpression AND down-regulated by its depletion (Figures 6a, yellow symbols on right side, and Figure 6d, yellow symbols on left side), and these were highly enriched in mitochondrial metabolic pathways (Figure 6g). A smaller number of genes (36) were down-regulated by *LINC00473* overexpression AND up-regulated by *LINC00473* depletion, and these genes enriched pathways related to extracellular matrix composition (Figure 6h). Importantly, the expression levels of overlapping *PDE10* transcripts were not affected in adipocytes with overexpression or knockdown of *LINC00473* (Supplementary Tables 5 and 6, and Supplementary Figure 3) Together with subcellular localization and functional studies these results support the hypothesis that the primary site of *LINC00473* function is at the mitochondrial-lipid droplet interface through interactions that include PLIN1, and this function elicits feedback adaptations in gene expression that principally impact mitochondrial lipid oxidation.

Mechanisms controlling LINC00473 expression

To further explore the mechanisms by which LINC00473 expression might be controlled, we first examined its dependency on cAMP by inhibiting adenylyl cyclase activity (Figure 7a). Induction of LINC00473 was completely abolished by H89 inhibitor, placing it downstream of cAMP signaling. Moreover, the most significantly overrepresented GO molecular functions enriched in the set of genes most highly correlated with *LINC00473* (Figure 7b and Supplementary Table 7) were associated with cAMP signaling (Figure 7c, Supplementary Table 8). To further delineate the mechanisms by which cAMP signaling induces *LINC00473*, we studied transcription factors that are predicted to bind upstream of the transcription start site (CREB, ATF4, JUN and SP1). Of these, expression of *ATF4* and *JUN* was significantly stimulated and *SP1* was significantly inhibited by NE, as assessed by RNAseq (Figure 7d). To determine whether these alterations in transcription factor expression are functionally associated to LINC00473 induction, we performed siRNA mediated knockdown. Both mRNA and protein levels of these four factors were depleted by siRNA pools used (Figure 7e,f), but only *SP1* knockdown resulted in increased expression of *LINC00473* (Figure 7g). These results suggest that *LINC00473* is induced at least in part through cAMP-mediated suppression of *SP1*.

Discussion

In this paper we identify *LINC00473* as the gene most closely and specifically associated with development of human thermogenic adipocytes, involved in key energetic functions. *LINC00473* has been previously detected in humans²⁶ and has been catalogued as a functionally relevant sense intronic lncRNA in a comprehensive atlas of human long non-coding RNAs with accurate 5' ends²⁷. Previous reports by Chen *et al.*, who performed 5' and 3' rapid amplification of cDNA ends (RACE) assays and coding potential analysis of *LINC00473* supported its identity as a non-coding RNA with no protein coding potential²⁸. Using BLASTN 2.8.0+ against "NR" database we searched for orthologues of *LINC00473* across all species, and detected 243 homologs sequences in primates, but not in lower eukaryotes (Figure 8a). Species-specific expression of *LINC00473* is consistent with reports of rapid evolution in non-coding sequences with a nucleotide substitution of 90%, compared to a substitution rate of ~10% in protein-coding sequences²⁹. Other primate-specific lncRNAs involved in cholesterol levels in human liver³⁰, and in white adipocyte differentiation³¹, have been found, emphasizing the need for conducting studies on the function of lncRNAs involved in metabolism in a species-specific context. Because RNA can maintain a conserved secondary structure³², it is possible that functional orthologues of *LINC00473* and other metabolically important lncRNAs may exist in mice. Indeed, several lncRNAs have been identified as regulators of adipogenesis³³, and lncRNAs associated specifically with brown adipocytes have also been identified^{34–39}.

We investigated the specific role of *LINC00473* in thermogenic adipocyte development and function through analysis of its subcellular localization and identification of potential interacting targets. *LINC00473* is detected at low levels in the nucleus but is rapidly upregulated and transported to the cytoplasm upon elevation of cAMP. Thus, *LINC00473* may have both nuclear and cytoplasmic functions. A nuclear role for *LINC00473* in the

context of cAMP signaling has been reported^{28,40,41} interacting with NONO and cyclic AMP-responsive-element-binding protein (CREB)-regulated transcription coactivator (CRCT), which is essential in CREB transcriptional regulation²⁸. In the context of thermogenic adipocytes, CREB both directly and through interaction with NR4A3^{42–44} activates the *UCPI* promoter. Thus, when activated early in development, *LINC00473* may coordinate the actions of transcription factors that regulate *UCPI* expression.

In contrast to its nuclear localization in the basal state, *LINC00473* is strongly expressed and translocated to the cytoplasm in response to cAMP. Under these conditions, *LINC00473* can be crosslinked to both mitochondrial and lipid droplet proteins and localizes to the mitochondrial lipid droplet interphase. The localization of *LINC00473* to this region may help assemble the close association between mitochondria and lipid droplets (Figure 8b), that coordinates lipogenesis and lipolysis in thermogenic adipocytes^{45–47}. Alternatively, *LINC00473* may coordinate lipid droplet association during mitochondrial fission, which is necessary for catecholamine-induced respiration and thermogenic adipose tissue function^{45,46,48}.

Overexpression and depletion of *LINC00473* leads to corresponding increased- and decreased respiration and lipolytic responsiveness, and to changes in expression of genes associated with mitochondrial metabolic pathways, saliently lipid oxidation. It is likely that these changes in gene expression are secondary adaptative responses to primary effects of *LINC00473* on lipid droplet dynamics and mitochondrial activity, as genes in proximity to the *LINC00473* locus, particularly *PDE10* which could hypothetically influence cAMP mediated lipolytic activity, were not altered. Importantly, *LINC00473* expression is sensitive to lipid droplet dynamics, as depletion of PLIN1 led to a significant decrease in Fsk-stimulated *LINC00473* induction, associated with decreased lipolytic responsiveness. Thus, a tightly interactive network involving *LINC00473*, PLIN1 and mitochondrial lipid oxidation defines human thermogenic adipocyte energy metabolism (Figure 8b).

In summary, our work demonstrates that *LINC00473* is a functional marker of human thermogenic adipocytes, where, in response to cAMP it is induced and shuttled to the cytoplasm where it plays a role in coupling mitochondrial respiration and lipolysis through interactions at the mitochondrial-lipid droplet interphase. To the best of our knowledge this is the first example of a role for a long non-coding RNA in energy metabolism, a finding that provides insight into the complex mechanisms of metabolic signaling that underlie adipose tissue function, and their impairment in metabolic disease.

METHODS

Human Subjects

The study had two cohorts of patients, one of which was based at the UMass Memorial Health Care Center and the other was based at clinics of the Otorhinolaryngology, Head and Neck Surgery and Audiology Departments of Rigshospitalet / Gentofte Hospital and the Department of Otorhinolaryngology, Head, Neck and Maxillofacial Surgery, Zealand University Hospital of Copenhagen, Denmark. All study subjects were age of 23–82 (32% males), not pregnant or incarcerated. The clinical characteristics of the human subjects are

listed in Supplementary Table 1. All participants gave written informed consent. Both studies were performed according to the Declaration of Helsinki and NIH guidelines.

At the UMass Memorial Health Care Center, samples were collected from patients undergoing carotid endarterectomies and panniculectomies. In brief, carotid adipose tissue was collected by removing perivascular fat surrounding the carotid artery during carotid endarterectomies. Neck subcutaneous tissue was collected by sampling the subcutaneous adipose tissue approximately above the area where perivascular tissue was taken. Abdominal adipose tissue was collected from discarded tissues of patients undergoing panniculectomies. Tissue was harvested, placed in EGM-2 MV. Adipose tissue was then minced in 1mm pieces and embedded in Matrigel as detailed below. This study was approved by the University of Massachusetts Institutional Review Board, IRB H00001329.

At the Gentofte Hospital and the Zealand University Hospital of Copenhagen (Denmark), the human cohort is well-characterized and described in detail in Supplementary Table 1. In brief, 35 patients scheduled for surgery due to benign goiter were included in the main study, and 36 were additionally included in the biopsy part only. The material was collected from 2014 and October 2016 at the outpatient clinics of the Otorhinolaryngology, Head and Neck Surgery and Audiology Departments of Rigshospitalet / Gentofte Hospital and the Department of Otorhinolaryngology, Head, Neck and Maxillofacial Surgery, Zealand University Hospital of Copenhagen, Denmark. Apart from thyroid malignancy and inability to provide informed consent, there were no specific exclusion criterions. The Scientific-Ethics Committees of the Capital Region of Denmark approved the study protocol (HD-2009-020). The characteristics listed in Supplementary Table 1 includes the mean BMI, gender and age for the subjects included in the adipose tissue depot comparison presented in Figure 1g. A subgroup of 30 individuals were further examined for blood glucose levels after an Oral Glucose Tolerance Test (OGTT). One subject was excluded from the analysis due to high thyroid hormone levels. The characteristics for the remaining 29 subjects are presented Supplementary Table 1, last section. The subjects were divided into three BMI groups, normal weight (BMI < 25), overweight (BMI 25–30) and obese (BMI > 30) and a Type 2 diabetes group (T2DM). The four individuals in the T2DM group were classified based on the blood glucose levels in the OGTT (definition from the World Health Organization (WHO) ⁵⁰). The subcutaneous abdominal biopsies were obtained using a modified Bergström needle biopsy procedure as previously described after induction of general anesthesia and immediately prior to initiation of surgery. The supraclavicular biopsies were obtained by the surgeon from the deep neck fatty tissue depots as described previously ⁸. Biopsy samples were homogenized in TRIzol (Invitrogen, Carlsbad, CA, USA) using a TissueLyser (Qiagen, Valencia, CA, USA) and total RNA was then isolated as described in the method section “RNA isolation and reverse transcriptase for primary adipocytes cultures”.

Cell culture

Cell culture of human primary adipocytes from SVF—As previously described, preadipocytes were isolated from supraclavicular and abdominal subcutaneous adipose tissue biopsies ⁸. Biopsies were minced and digested in DMEM/F12 (containing collagenase

II (1 mg/ml; Sigma Aldrich) and fatty acid-free bovine serum albumin (15 mg/ml; Sigma Aldrich) for 20 min at 37 °C during gentle shaking. Following digestion, the suspension was filtered through a 70-micron cell strainer and left to settle for 5 min. The liquid phase below the upper lipid phase was aspirated using a syringe and passed through a 30-micron filter. The cell suspension was spun down at 800 g for 7 min and washed with DMEM/F12. Preadipocytes were resuspended in DMEM/F12, 1% penicillin/streptomycin, 10% fetal bovine serum (FBS) (Life technologies) and seeded in a 5-ml culture flask. Media was changed the day after isolation and then every second day until cells were 80% confluent and then split into a 10-cm dish (passage 1). For the cell experiments, preadipocytes were cultured in 100 mm and 6 cm culture dishes containing DMEM/F12, 10% FBS, 1% Penicillin-Streptomycin (all from Invitrogen) and 1 nM Fibroblast growth factor-acidic (FGF-1) (ImmunoTools). The cells were grown at 37°C in an atmosphere of 5% CO₂ and the medium was changed every second day. Adipocyte differentiation was induced two days after preadipocyte cultures were 100% confluent by treating cells with DMEM/F12 containing 1% Penicillin-Streptomycin, 0.1 μM dexamethasone (Sigma-Aldrich), 100 nM insulin (Actrapid, Novo Nordisk or Humulin, Eli Lilly), 200 nM rosiglitazone (Sigma-Aldrich), 540 μM isobutylmethylxanthine (IBMX) (Sigma-Aldrich), 2 nM T3 (Sigma-Aldrich) and 10 μg/ml transferrin (Sigma-Aldrich). After three days of differentiation, IBMX was removed from the cell culture media. The cell cultures were left to differentiate for an additional nine days, with medium change the third day. Following 12 days of differentiation, cells were harvested for RNA, protein. When stated in the figure legend, cells were stimulated with 10 μM norepinephrine (Sigma-Aldrich) for 4 hr before RNA and protein were isolated. Two hours prior to the norepinephrine stimulation, old medium was replaced by DMEM/F12 (Life technologies) containing 1% penicillin-streptomycin.

Cell culture of progenitor cells derived from human adipose explants—We collected carotid perivascular and neck subcutaneous adipose tissues from carotid endarterectomies with no a-priori selection of individual donors. The characteristics of patients from which tissues were used for indicated experiments are described in Supplementary Table 1. Detailed methods for culture of adipose tissue explants and harvesting of single cells from explant growth are published⁵¹. In brief, cell suspensions from capillary growth were obtained using dispase, and plated on standard tissue culture plates. Growth and passaging of these cells was done using EGM-2 MV. To induce adipogenesis we used a minimal adipogenic cocktail of DMEM +10% FBS, 0.5 mM 3-isobutyl-1-methylxanthine, 1μM dexamethasone, and 1μg/ml insulin (MDI) for 72h. The medium was then replaced with DMEM plus 10% FBS. Subsequently, 50% of the medium was replaced with fresh medium every other day. Adipocyte markers were measured by RT-PCR in RNA extracted from 3 explants per condition.

Cell culture of additional cell lines for analysis of LINC00473 expression—Four different human cell types, responsive to norepinephrine was selected. 1) Human satellite cells were isolated from vastus lateralis muscle biopsies and then differentiated to multinuclear myotubes as previously described (PMID: 21911750). 2) Human Cardiac Myocytes (C-12810) and 3) Human Pulmonary Artery Smooth Muscle Cells (C-12521) cells were Purchased from Promo Cell (. The cells were cultured and differentiated according to

Promo Cells standard protocols. 4) Human Thermogenic adipocytes isolated from the supraclavicular region. Cells were cultured and differentiated as described in Promo Cells standard protocols. All four cell types were incubated with 10 μ M norepinephrine for 4 hours before harvested with TRIzol. cDNA synthesis and qPCR were performed as previously described.

Other methods

Bodipy staining—Fully differentiated adipocytes were fixed in 4% Formaldehyde for 15 min and washed with DPBS (Gibco) three times. Bodipy (Thermo Fisher) was diluted in HBSS to a final concentration at 0.5mM and incubated with fixed cells for 20 min. After washing with DPBS, 1 drop NucBlue™ Fixed Cell ReadyProbes™ Reagent (Thermo Fisher) pr. ml HBSS was added for staining of the nucleus (8 min incubation). Pictures of cells were taken with EVOS Auto microscope (Thermo Fisher).

RNA isolation and reverse transcription for primary adipocytes cultures—Total RNA (200 ng) was reverse transcribed using cDNA high capacity kit (Applied Biosystems) according to the manufacturer's protocol. cDNA samples were loaded in triplicates and qPCR was performed using ViiA7 Sequence Detection system (Applied Biosystems, Foster City, CA, USA) according to the manufacturer's protocol using either PowerUp SYBR Green Master Mix (Thermo Fisher) or TaqMan™ Universal PCR Master Mix (Thermo Fisher). SYBR based primers were designed using Roche Applied Science Assay Design Center (Roche) and checked for specificity using Primer-Blast (NCBI)

RNA-Sequencing—RNA (1000 ng) was extracted from adipocytes using the Trizol method. RNA sequencing was performed by BGI (Hong Kong) using 1000 ng RNA for the TruSeq cDNA library construction (Illumina). 3Gb data was generated per sample on a HiSeq 2000 sequencer (Illumina). A 91-paired end sequencing strategy was used for the project. Overall read quality was assessed using FastQC <http://www.bioinformatics.babraham.ac.uk> and the following pre-processing steps were performed using the Fastx toolkit (<http://hannonlab.cshl.edu>) and PRINSEQ: 7 nt were clipped off from the 5' end of every read⁵². The reads were then filtered to remove all N-reads. The 3' ends were then trimmed and the reads filtered to minimum Q25 and 50 bp length. Reads were then mapped with tophat2 to the human genome GRCh38 Ensembl release 77⁵³. Read counts were imported into R, and DESeq2 was used for identifying differential expression⁵⁴, as implemented in DEBrowser⁵⁵. For the isoform analysis, fpkm values from cufflinks were used^{56,57}.

RNA extraction of cells derived from human adipose explants—The media was aspirated from the well and cells were washed 2X with PBS. TriPure Trizol reagent was added to the cells and incubated at room temperature for 5 minutes. Cells were collected into a GentleMACS M tube and dissociated using the GentleMACS Dissociator (Miltenyi Bio) Program RNA01.01. Tubes were centrifuged for 3 minutes at 800RPM and the mixture was transferred to a 2ml collection tube. Chloroform was added in a 1:5 ratio to the tripure/cell mix and tubes were inverted to mix, then incubated at room temperature for 3–5 minutes. Aqueous phase separation was performed, and the RNA-containing layer was mixed with an

equal volume of 100% Isopropanol and incubated overnight at -20 degrees for precipitation. RNA was pelleted and washed with 80% ETOH and eluted in nuclease-free water. Nucleotide concentrations were determined using Nanodrop 2000. $1\mu\text{g}$ of RNA was reverse transcribed using iScript cDNA Synthesis Kit (BioRad).

Affymetrix arrays—Total RNA was isolated using TRIzol as above. Affymetrix protocols were followed for the preparation of cRNA, which was hybridized to HTA-2.0 arrays. Raw expression data collected from an Affymetrix HP GeneArrayScanner was normalized across all data sets using the RMA algorithm as implemented by the Affymetrix Expression Console. Expression analysis was performed using the Affymetrix Transcriptome Analysis Console v.3.0.

Cell fractionation—Human preadipocytes were seeded at a density of 3×10^6 cells per plate into three 10cm plates per condition and grown to confluence for 72h. Plates were differentiated with MDI media for a total of 7 days (see differentiation protocol). Six hours prior to collection one half of the plates were stimulated with 10uM Forskolin (Sigma, F3917). Cells were collected by trypsinization and washed 1x with PBS. Cells were pelleted and stored at -80°C overnight. Cells were then re-suspended into 2ml of cracking buffer (50mM Hepes pH 7.9, 3mM MgCl_2 , 1mM DTT, 0.25M Sucrose, 40U/ml RNase-out). and broken by 10 passages through successively smaller bore needles (18, 22, 25 and 27g). Homogenates were centrifuged at $400 \times g$ for 10 minutes at 4°C yielding Pellet 1 (unbroken cells, nuclei), and resulting supernatant centrifuged at $700 \times g$ for 5 minutes yielding Pellet 2, (mitochondria and nuclei); resulting supernatant was centrifuged at $20,000 \times g$ for 5 minutes yielding Pellet 3, (heavy mitochondria), and resulting supernatant centrifuged at $20,000 \times g$ for 20 minutes yielding Pellet 4 (light mitochondria) and Supernatant A (Cytoplasm). For collection of the fat cake, the homogenate was directly centrifuged at $20,000 \times g$ for 20 minutes and the floating fat cake and supernatant removed for analysis.

Mass Spectrometry—Cells were cultured, differentiated, treated and homogenized as described above. The supernatants from the second centrifugation step were pipetted into wells of a 6 well dish kept on ice, and UV-crosslinked at an intensity of $0.5\text{J}/\text{cm}^2$. Crosslinked extracts were mixed with equal volumes of 2x hybridization buffer composed of 20 mM Tris-HCl pH 7.5 (Life Technologies #15567-027), 10 mM EDTA (Life Technologies #15575-020), 1M LiCl (Sigma #L7026), 1% dodecyl maltoside (DDM, Sigma #D4641), 0.4% sodium dodecyl sulfate (SDS, Ambion #AM9820) 0.2% sodium deoxycholate (Sigma #06750), 8 M urea (Sigma #U0631-500G) and 5mM Tris(2-carboxyethyl)phosphine (TCEP, Sigma #646547). Extracts were pre-cleared by incubating for 30 min at 37°C with constant mixing with Streptavidin-coated magnetic beads (Life Technologies, Dynabeads MyOne C1 #65002), previously washed 2 times with hybridization buffer. After removal of the beads, extracts were incubated for 4 hours at 37°C with constant mixing with a probe mixture composed of 13 biotinylated probes (gtgcttgctctcaggaac; cagcaactcggactcagac; atcttctcgcaaaaggcgag; aactcgcgcaagcaagttgc; aagtatgctgacgcgcatat; cgcagttttcatcgtgatg; aggccgagcataaagtagta; cagggttgcccaataaac; tccgcttgcattcagaata; gtaaaccitacacctgaca; gagaatcccgcacaaccaag; gaaaaccctcagaaggagg; tatgacttgggttctctgg (Biosearch)) each at a final concentration of $5\mu\text{M}$. Probes were previously denatured by heating to 85°C for 3 min.

Probes were subsequently captured by incubation with streptavidin-coated magnetic beads for 30 min at 37 °C with constant mixing, followed by magnetic separation. Beads were washed 5 times with 2x bead volume of hybridization buffer for 5 min per wash and stored at –80°C until elution and mass spectrometry analysis. Proteins were digested on beads by adding 100 µl digestion buffer (2M urea in 50 mM Tris pH 8.5, 1 mM DTT and 150 ng of Tpsin). Beads were incubated for 1h on shaker at room temperature. After 1 h, the samples were centrifuged at 2000 rpm for 5 min, supernatant was removed, 5 mM of chloracetamid was added and proteins were digested overnight at 37 degrees. The following day, peptides were acidified by addition of trifluoroacetic acid and purified on styrenedivinylbenzene reverse phase sulphonate (SDP RPS). For the mass spectrometry analysis, peptides were separated on RP ReproSil-Pur C18-AQ 3 µm resin (Dr. Maisch) columns (15 cm) and injected into an Orbitrap mass spectrometer (Q Exactive HFX, Thermo Scientific, Germany, 58). Raw data was analyzed with MaxQuant software using label free algorithm⁵⁹. To define protein groups specifically associated with LINC00473, we leveraged the fact that there is virtually absent in the absence of Fsk stimulation; thus the ratio of LFQ values for each protein group from samples incubated with or without Fsk, in pulldowns using specific probes versus no probes were considered. The top 50 proteins ranked by the ratio of +Fsk/-Fsk are shown in Figure 4.

Immunoprecipitation of crosslinked extracts—Four independent cell experiments using differentiated adipocytes from four different human donors were included. Each experiment consisted of a 4h 10 µM norepinephrine stimulation and a control stimulation. Before the IP procedure, cells were incubated with 2% formaldehyde solution for 15 min at RT. After washing with PBS, cells were lysed and incubated overnight at 4°C in a RIP Washing buffer containing EDTA, RNase Inhibitor and 1:50 diluted PLIN1 antibody (CST #9349) conjugated to A/G Protein magnetic beads. As the negative control a purified Rabbit IgG (Merc Millipore: PP64B) was utilized. After incubation, tubes were placed on a magnetic separator (Merc Millipore), supernatants were discarded, and magnetic beads bound to PLIN1 protein and *LINC00473* were washed in RIP washing buffer. A solution consisting of RIP washing buffer, Proteinase K and SDS was added the magnetic beads precipitate and placed in a 55°C warm heating block for 30 minutes. Tubes were vortexed for 5 seconds every 3rd minute during the heat incubation. Tubes were then placed on the magnetic separator and the supernatant was removed to a new tube. RNA from this fraction was isolated using two separated phase separation steps with phenol:chloroform:isoamyl solution (Sigma Aldrich) and chloroform, respectively. The RNA was then precipitated using two salt solutions (Merck Millipore: CS203173 & CS203185) a precipitate enhancer (Merck Millipore: CS203208) and absolute ethanol. Samples were then frozen at –80°C overnight before centrifugation at 15000 RPM for 30 minutes. RNA was washed with 80% ethanol twice before dissolving RNA pellet in 15 µl RNase free H₂O. For the cDNA synthesis a 20 ng RNA input was used, using the same cDNA kit as described in the section “RNA isolation and reverse transcriptase for primary adipocytes cultures.”

Microscopy—*LINC00473* localization was visualized using the RNAscope multiplex fluorescent assay kit (ACD Bio, 320851). Cells were seeded on 1.5mm thick coverslips inside 24 well tissue culture dishes at a density of 1×10⁵ cells per well. Cells were grown

to confluency and differentiated with MDI media as described above. At day 7 of differentiation cells were simulated with 10 μ M forskolin for 6 hours, fixed with 4% PFA for 15 minutes at room temperature and dehydrated with increasing concentrations of EtOH. Coverslips were stored in 100% EtOH at -20°C for up to one week. RNAscope was performed using a target probe to LINC00473 (ACD Bio, 464821) according to manufacturer's protocol. Immunofluorescent staining was performed following the completion of the RNAscope protocol, by overnight incubation with anti-HSP70 (1:200) (Invitrogen, MA3-028) and anti-perilipin (1:200) (Abcam, ab61682) antibody at 4°C in permeabilization buffer containing 1% FBS and 0.5% Triton X in 1x PBS. Coverslips were washed 3 times in permeabilization buffer and incubated at room temperature with species matched secondary antibody (1:1000) for 30 minutes. Three washes were performed before the coverslips were stained with hoechst (DAPI)(1:1000) and mounted with ProLong Gold antifade reagent. Cells were visualized on a Zeiss Axiovert 200M inverted microscope or a Leica TCS SP8 with LIGHTNING super-resolution. Image analysis was done using ImageJ (FIJI) software. To assess colocalization, we used ImageJ/FIJI software. All images subjected to comparison were assembled into a composite, and all image filtering was performed on the composite to control for any quantitative effect of filtering introduced by operator bias. After background subtraction and binary thresholding the number and size of particles in each channel for each image was assessed using the particle counting feature in Fiji/ImageJ. The amount of overlap between channels was calculated by measuring the arithmetic product of binary images, relative to each image. To determine spurious overlap the same operation was performed using content-rich image sections flipped along the horizontal axes. Means from 8–10 independent images were used.

Gene silencing—For silencing of *LINC00473* adipocytes were transfected using siRNA pools consisting of four siRNA oligos specifically targeting four different sites of target *LINC00473* (On Target Plus, R-032718-00-0005, Dharmacon). Transfections were performed using 10 μ l Lipofectamine® RNAiMAX Transfection Reagent (Thermo Fisher Scientific) with 20 nM of siRNA, at day 11 of differentiation in antibiotic-free cell culture media (Opti-MEM®, F12/DMEM) for 24h. A scrambled non-specific oligonucleotide (siRNA Scr) was used as control. For silencing of transcription factors, the online webtool TFBIND⁶⁰ was used to estimate the transcription factor DNA binding probability 5000 kb upstream of LINC00473 TSS. The list of potential transcription factors was screened in the RNA-sequencing data included in this manuscript. The four most likely Transcription factors (CREB1, ATF4, JUN, and SP1) were selected for further analysis, based on the expression levels. Dharmacon ON-TARGETplus Non-targeting Pool knock down probes were used to silence the expression of the four transcripts at day 0 in the differentiation program. RNA was harvested at day 12 after a four-hour NE-stimulation. For western blotting, protein was extracted from adipocytes using Radioimmunoprecipitation (RIPA) buffer (150 mM NaCl, 1% NP40, 0.5% sodium deoxycholate, 0.1% SDS, 1 mM EDTA, 50 mM Tris pH 7.5) containing protease inhibitor cocktail (S8820-20TAB; Sigma-Aldrich). Protein concentration was determined using the Pierce BCA protein assay kit (Thermo Scientific). Proteins were separated using 4–12% Criterion™ XT Bis-Tris Protein Gels (BioRad #3450124) and transferred to PVDF membranes. Blots were incubated overnight at 4°C in the following primary antibodies: SP1 (CST #9389), ATF4 (CST #11815), c-JUN

(CST #9165), CREB (CST #9197), and Vinculin (loading control; Bionordika 13901S). Following incubation with primary antibodies, membranes were incubated in Goat anti-rabbit IgG HRP Conjugate (BioRad #170–6515) for one hour and developed using Luminata Forte Western HRP Substrate (Millipore #WBLUF0100). For silencing of *PLIN1*, cells were transfected at day 5 of differentiation using three individual oligos described in Supplementary Table 9, and analyzed 48h later.

Overexpression of *LINC00473* in primary adipocytes using CRISPR-SAM—

Immortalized human white adipose progenitor cells derived from human neck fat and stably expressing the dCasp-VP64 and MS2-P65-HSF1 components of the CRISPR-SAM system^{61,62} were transduced with either an empty vector (EV) lentivirus solution as control or with lentivirus carrying the sgRNA targeting the promoter region of *LINC00473*, as previously described⁶³. Selection of sgRNA-expressing cells was done using Zeocin (final concentration of 50 mg/ml). Zeocin was kept in media during passaging of the cell lines. Confirmation of *LINC00473* overexpression (OE) was done in differentiated adipocytes using qPCR. Seven different sgRNA were tested for OE. Guide 6 +20kb from TSS were markedly more efficient than the other guide RNAs (Supplementary Table 9). The guide 6-expressing (Gd6) and control preadipocytes were grown in high-glucose Dulbecco's modified Eagle's medium (DMEM/H) supplemented with 10% (vol/vol) fetal bovine serum (FBS) and 1% penicillin-streptomycin⁶⁴. For adipocyte differentiation, cells were grown to confluence for 6 days and then exposed to adipogenic induction mixture in DMEM/H medium containing 0.5 mM isobutylmethylxanthine, 0.1 mM dexamethasone, 0.5 mM human insulin (Sigma Aldrich), 2 nM T3, 30 mM indomethacin, 17 mM pantothenate, 33 mM biotin and 2% FBS for another 12 days. Induction medium was changed every 3 days until cells were collected.

Oxygen consumption—Oxygen consumption was measured using a Seahorse Bioscience XF96 Extracellular Flux Analyser according to the manufacturer's protocol. Adipocytes were grown until reaching 100% confluency and were then seeded in seahorse plates at a 1:1 ratio, and differentiated as described above. Experiments were performed on day 12 of differentiation on cells in passage three and Knock down experiments were performed as described above. Oxygen consumption rate was assessed in 4 primary brown adipocyte cultures. The results were extracted from the Seahorse Program Wave 2.2.0. Baseline measurements of OCR were performed for 30 minutes before NE or saline was added and measurements of the concomitant responses were recorded for 60 minutes. All other states were induced using the seahorse XF cell mito stress test kit according to the manufacturer's protocol. After 90 minutes, leak state was induced by adding Oligomycin, which inhibits the ATP synthase. Leak state measurements were performed for 20 minutes, then the ionophore (carbonyl cyanide-4-(trifluoromethoxy) phenylhydrazone) (FCCP), which collapses the proton gradient across the mitochondrial inner membrane resulting in a completely uncoupled state. After an additional 20 minutes Antimycin A and Rotenone were added to inhibit complexes III and I respectively, resulting in only non-mitochondrial respiration. For data analyses OCR was corrected for non-mitochondrial respiration as assessed by the Seahorse XF cell mitochondrial stress test kit. Wells were excluded from the data analyses if OCR were +/-20% of the mean in that series of replicate values.

NEFA Assay—Cells were incubated 300 μ l DMEM/F12 media (Gibco) with 10 μ M Forskolin added 5% Bovine Serum Albumin (Free fatty Acid Free). After 6 hours incubation, the media was removed and stored at -80°C until further analysis. 10 μ l media was used for the free fatty acid quantification using the NEFA assay (WAKO), an *in vitro* enzymatic colorimetric method assay for quantitative determination of non-esterified fatty acids (NEFA) in cultured media. A NEFA standard (WAKO) was used to generate the standard curve. The assay was performed in NUNC F96 Immuno plates and data collected in a Sunrise Plate reader at 550 nm.

QUANTIFICATION AND STATISTICAL ANALYSIS

GraphPad Prism 7.0 was used for all analyses. Parametric or non-parametric test were chosen based on results from the D'Agostino-Pearson omnibus normality test and are described in each figure. Heat maps were plotted using Morpheus (Broad Institute).

DATA AVAILABILITY STATEMENT

Sequences of all oligonucleotides used in this study are in Supplementary Table 9. Further information and requests for resources and reagents should be directed to and will be fulfilled by Silvia Corvera (silvia.corvera@umassmed.edu)

Supplementary Material

Refer to Web version on PubMed Central for supplementary material.

Acknowledgements

This study was supported by NIH grant DK089101-04 to SC. We acknowledge the use of services from the UMASS Bioinformatics Core, supported by NIH CTSA grant UL1 TR000161-05, and from the UMASS SCOPE core for high resolution confocal imaging. KVT was supported by NIH grant 5T32HL120823-03. The Centre for Physical Activity Research (CFAS) is supported by a grant from TrygFonden (Grants ID 101390 and ID 20045). During the study period, the Centre of Inflammation and Metabolism (CIM) was supported by a grant from the Danish National Research Foundation (DNRF55). SN was further supported by the Danish Council for Independent Research, Medical Sciences (4092-00492B). NZJ, CNB and TJ were funded by Danish Diabetes Academy supported by the Novo Nordisk Foundation. EB, BE & ML were supported by internal funding from the Novo Nordisk Foundation Center for Basic Metabolic Research, an independent research center at the University of Copenhagen partially funded by an unrestricted donation from the Novo Nordisk Foundation (NNF18CC0034900).

REFERENCES

1. Rosen ED & Spiegelman BM Adipocytes as regulators of energy balance and glucose homeostasis. *Nature* 444, 847–853 (2006). [PubMed: 17167472]
2. Harms M & Seale P Brown and beige fat: development, function and therapeutic potential. *Nat Med* 19, 1252–1263 (2013). [PubMed: 24100998]
3. Nedergaard J & Cannon B The changed metabolic world with human brown adipose tissue: therapeutic visions. *Cell Metab* 11, 268–272 (2010). [PubMed: 20374959]
4. Crewe C, An YA & Scherer PE The ominous triad of adipose tissue dysfunction: inflammation, fibrosis, and impaired angiogenesis. *J Clin Invest* 127, 74–82 (2017). [PubMed: 28045400]
5. Deshmukh AS, et al. Proteomics-Based Comparative Mapping of the Secretomes of Human Brown and White Adipocytes Reveals EPDR1 as a Novel Adipokine. *Cell Metab* 30, 963–975 e967 (2019). [PubMed: 31668873]

6. Cypess AM, et al. Anatomical localization, gene expression profiling and functional characterization of adult human neck brown fat. *Nat Med* 19, 635–639 (2013). [PubMed: 23603815]
7. Virtanen KA, et al. Functional brown adipose tissue in healthy adults. *N Engl J Med* 360, 1518–1525 (2009). [PubMed: 19357407]
8. Jespersen NZ, et al. A classical brown adipose tissue mRNA signature partly overlaps with brite in the supraclavicular region of adult humans. *Cell Metab* 17, 798–805 (2013). [PubMed: 23663743]
9. Jespersen NZ, et al. Heterogeneity in the perirenal region of humans suggests presence of dormant brown adipose tissue that contains brown fat precursor cells. *Mol Metab* 24, 30–43 (2019). [PubMed: 31079959]
10. Min SY, et al. Human ‘brite/beige’ adipocytes develop from capillary networks, and their implantation improves metabolic homeostasis in mice. *Nat Med* 22, 312–318 (2016). [PubMed: 26808348]
11. Sanchez-Gurmaches J, Hung CM & Guertin DA Emerging Complexities in Adipocyte Origins and Identity. *Trends Cell Biol* 26, 313–326 (2016). [PubMed: 26874575]
12. Tran KV, et al. The vascular endothelium of the adipose tissue gives rise to both white and brown fat cells. *Cell Metab* 15, 222–229 (2012). [PubMed: 22326223]
13. Berry R & Rodeheffer MS Characterization of the adipocyte cellular lineage in vivo. *Nat Cell Biol* 15, 302–308 (2013). [PubMed: 23434825]
14. Jeffery E, et al. The Adipose Tissue Microenvironment Regulates Depot-Specific Adipogenesis in Obesity. *Cell Metab* 24, 142–150 (2016). [PubMed: 27320063]
15. Mercer T, Dinger M & Mattick J Long non-coding RNAs: insights into functions. *Nat Rev Genet* 10, 155–159 (2009). [PubMed: 19188922]
16. Engreitz JM, Ollikainen N & Guttman M Long non-coding RNAs: spatial amplifiers that control nuclear structure and gene expression. *Nat Rev Mol Cell Biol* 17, 756–770 (2016). [PubMed: 27780979]
17. Ransohoff JD, Wei Y & Khavari PA The functions and unique features of long intergenic non-coding RNA. *Nat Rev Mol Cell Biol* 19, 143–157 (2018). [PubMed: 29138516]
18. Zhao XY, Li S, Wang GX, Yu Q & Lin JD A long noncoding RNA transcriptional regulatory circuit drives thermogenic adipocyte differentiation. *Mol Cell* 55, 372–382 (2014). [PubMed: 25002143]
19. Alvarez-Dominguez JR, et al. De Novo Reconstruction of Adipose Tissue Transcriptomes Reveals Long Non-coding RNA Regulators of Brown Adipocyte Development. *Cell Metab* 21, 764–776 (2015). [PubMed: 25921091]
20. Bai Z, et al. Dynamic transcriptome changes during adipose tissue energy expenditure reveal critical roles for long noncoding RNA regulators. *PLoS Biol* 15, e2002176 (2017). [PubMed: 28763438]
21. Min SY, et al. Diverse repertoire of human adipocyte subtypes develops from transcriptionally distinct mesenchymal progenitor cells. *Proc Natl Acad Sci U S A* 116, 17970–17979 (2019). [PubMed: 31420514]
22. Nedergaard J, Bengtsson T & Cannon B Three years with adult human brown adipose tissue. *Ann N Y Acad Sci* 1212, E20–36 (2010). [PubMed: 21375707]
23. Sidossis LS, et al. Browning of Subcutaneous White Adipose Tissue in Humans after Severe Adrenergic Stress. *Cell Metab* 22, 219–227 (2015). [PubMed: 26244931]
24. Patsouris D, et al. Burn Induces Browning of the Subcutaneous White Adipose Tissue in Mice and Humans. *Cell Rep* 13, 1538–1544 (2015). [PubMed: 26586436]
25. Muppurala UK, Honavar VG & Dobbs D Predicting RNA-protein interactions using only sequence information. *BMC Bioinformatics* 12, 489 (2011). [PubMed: 22192482]
26. Fagerberg L, et al. Analysis of the human tissue-specific expression by genome-wide integration of transcriptomics and antibody-based proteomics. *Mol Cell Proteomics* 13, 397–406 (2014). [PubMed: 24309898]
27. Hon CC, et al. An atlas of human long non-coding RNAs with accurate 5’ ends. *Nature* 543, 199–204 (2017). [PubMed: 28241135]

28. Chen Z, et al. cAMP/CREB-regulated LINC00473 marks LKB1-inactivated lung cancer and mediates tumor growth. *J Clin Invest* 126, 2267–2279 (2016). [PubMed: 27140397]
29. Ward M, McEwan C, Mills JD & Janitz M Conservation and tissue-specific transcription patterns of long noncoding RNAs. *J Hum Transcr* 1, 2–9 (2015). [PubMed: 27335896]
30. Le Bras A The lncRNA CHROME regulates cholesterol homeostasis. *Nat Rev Cardiol* (2019).
31. Zhang X, et al. Interrogation of nonconserved human adipose lincRNAs identifies a regulatory role of linc-ADAL in adipocyte metabolism. *Sci Transl Med* 10(2018).
32. Torarinsson E, Sawera M, Havgaard JH, Fredholm M & Gorodkin J Thousands of corresponding human and mouse genomic regions unalignable in primary sequence contain common RNA structure. *Genome Res* 16, 885–889 (2006). [PubMed: 16751343]
33. Sun L, et al. Long noncoding RNAs regulate adipogenesis. *Proc Natl Acad Sci U S A* 110, 3387–3392 (2013). [PubMed: 23401553]
34. Xiong Y, et al. A novel brown adipocyte-enriched long non-coding RNA that is required for brown adipocyte differentiation and sufficient to drive thermogenic gene program in white adipocytes. *Biochim Biophys Acta* 1863, 409–419 (2018).
35. Nuermairaiti N, et al. Effect of lncRNA HOXA11-AS1 on adipocyte differentiation in human adipose-derived stem cells. *Biochem Biophys Res Commun* 495, 1878–1884 (2018). [PubMed: 29217197]
36. Liu W, et al. LncRNA Gm15290 sponges miR-27b to promote PPARgamma-induced fat deposition and contribute to body weight gain in mice. *Biochem Biophys Res Commun* 493, 1168–1175 (2017). [PubMed: 28943435]
37. Li M, et al. Long non-coding RNA ADNCR suppresses adipogenic differentiation by targeting miR-204. *Biochim Biophys Acta* 1859, 871–882 (2016). [PubMed: 27156885]
38. Xiao T, et al. Long Noncoding RNA ADINR Regulates Adipogenesis by Transcriptionally Activating C/EBPalpha. *Stem Cell Reports* 5, 856–865 (2015). [PubMed: 26489893]
39. Schmidt E, et al. LincRNA H19 protects from dietary obesity by constraining expression of monoallelic genes in brown fat. *Nat Commun* 9, 3622 (2018). [PubMed: 30190464]
40. Pruunsild P, Bengtson CP & Bading H Networks of Cultured iPSC-Derived Neurons Reveal the Human Synaptic Activity-Regulated Adaptive Gene Program. *Cell Rep* 18, 122–135 (2017). [PubMed: 28052243]
41. Liang XH, et al. Non-coding RNA LINC00473 mediates decidualization of human endometrial stromal cells in response to cAMP signaling. *Sci Rep* 6, 22744 (2016). [PubMed: 26947914]
42. Cannon B & Nedergaard J Brown adipose tissue: function and physiological significance. *Physiol Rev* 84, 277–359 (2004). [PubMed: 14715917]
43. Kozak U, et al. An upstream enhancer regulating brown-fat-specific expression of the mitochondrial uncoupling protein gene. *Mol Cell Biol* 14, 59–67 (1994). [PubMed: 8264627]
44. Yubero P, et al. Dominant negative regulation by c-Jun of transcription of the uncoupling protein-1 gene through a proximal cAMP-regulatory element: a mechanism for repressing basal and norepinephrine-induced expression of the gene before brown adipocyte differentiation. *Mol Endocrinol* 12 1023–1037 (1998). [PubMed: 9658406]
45. Benador IY, et al. Mitochondria Bound to Lipid Droplets Have Unique Bioenergetics, Composition, and Dynamics that Support Lipid Droplet Expansion. *Cell Metab* 27, 869–885 e866 (2018). [PubMed: 29617645]
46. Boutant M, et al. Mfn2 is critical for brown adipose tissue thermogenic function. *EMBO J* 36, 1543–1558 (2017). [PubMed: 28348166]
47. Yu J, et al. Lipid droplet remodeling and interaction with mitochondria in mouse brown adipose tissue during cold treatment. *Biochim Biophys Acta* 1853, 918–928 (2015). [PubMed: 25655664]
48. Wikstrom JD, et al. Hormone-induced mitochondrial fission is utilized by brown adipocytes as an amplification pathway for energy expenditure. *EMBO J* 33, 418–436 (2014). [PubMed: 24431221]

METHODS-REFERENCES

49. Kaimal V, Bardes EE, Tabar SC, Jegga AG & Aronow BJ ToppCluster: a multiple gene list feature analyzer for comparative enrichment clustering and network-based dissection of biological systems. *Nucleic Acids Res* 38, W96–102 (2010). [PubMed: 20484371]
50. Pedersen M, et al. Cognitive functions in middle aged individuals are related to metabolic disturbances and aerobic capacity: a cross-sectional study. *PLoS One* 7, e51132 (2012). [PubMed: 23251434]
51. Rojas-Rodriguez R, et al. Adipose tissue angiogenesis assay. *Methods Enzymol* 537, 75–91 (2014). [PubMed: 24480342]
52. Schmieder R & Edwards R Quality control and preprocessing of metagenomic datasets. *Bioinformatics* 27, 863–864 (2011). [PubMed: 21278185]
53. Kim D, et al. TopHat2: accurate alignment of transcriptomes in the presence of insertions, deletions and gene fusions. *Genome Biol* 14, R36 (2013). [PubMed: 23618408]
54. Love MI, Huber W & Anders S Moderated estimation of fold change and dispersion for RNA-seq data with DESeq2. *Genome Biol* 15, 550 (2014). [PubMed: 25516281]
55. Kucukural A, Yukselen O, Ozata DM, Moore MJ & Garber M DEBrowser: interactive differential expression analysis and visualization tool for count data. *BMC Genomics* 20, 6 (2019). [PubMed: 30611200]
56. Trapnell C, et al. Transcript assembly and quantification by RNA-Seq reveals unannotated transcripts and isoform switching during cell differentiation. *Nat Biotechnol* 28, 511–515 (2010). [PubMed: 20436464]
57. Roberts A, Trapnell C, Donaghey J, Rinn JL & Pachter L Improving RNA-Seq expression estimates by correcting for fragment bias. *Genome Biol* 12, R22 (2011). [PubMed: 21410973]
58. Kelstrup CD, et al. Limits for Resolving Isobaric Tandem Mass Tag Reporter Ions Using Phase-Constrained Spectrum Deconvolution. *J Proteome Res* 17, 4008–4016 (2018). [PubMed: 30220210]
59. Tyanova S, Temu T & Cox J The MaxQuant computational platform for mass spectrometry-based shotgun proteomics. *Nat Protoc* 11, 2301–2319 (2016). [PubMed: 27809316]
60. Tsunoda T & Takagi T Estimating transcription factor bindability on DNA. *Bioinformatics* 15, 622–630 (1999). [PubMed: 10487870]
61. Sustarsic EG, et al. Cardiolipin Synthesis in Brown and Beige Fat Mitochondria Is Essential for Systemic Energy Homeostasis. *Cell Metab* 28, 159–174 e111 (2018). [PubMed: 29861389]
62. Konermann S, et al. Genome-scale transcriptional activation by an engineered CRISPR-Cas9 complex. *Nature* 517, 583–588 (2015). [PubMed: 25494202]
63. Lundh M, Plucinska K, Isidor MS, Petersen PSS & Emanuelli B Bidirectional manipulation of gene expression in adipocytes using CRISPRa and siRNA. *Mol Metab* 6, 1313–1320 (2017). [PubMed: 29031730]
64. Xue R, et al. Clonal analyses and gene profiling identify genetic biomarkers of the thermogenic potential of human brown and white preadipocytes. *Nat Med* 21, 760–768 (2015). [PubMed: 26076036]

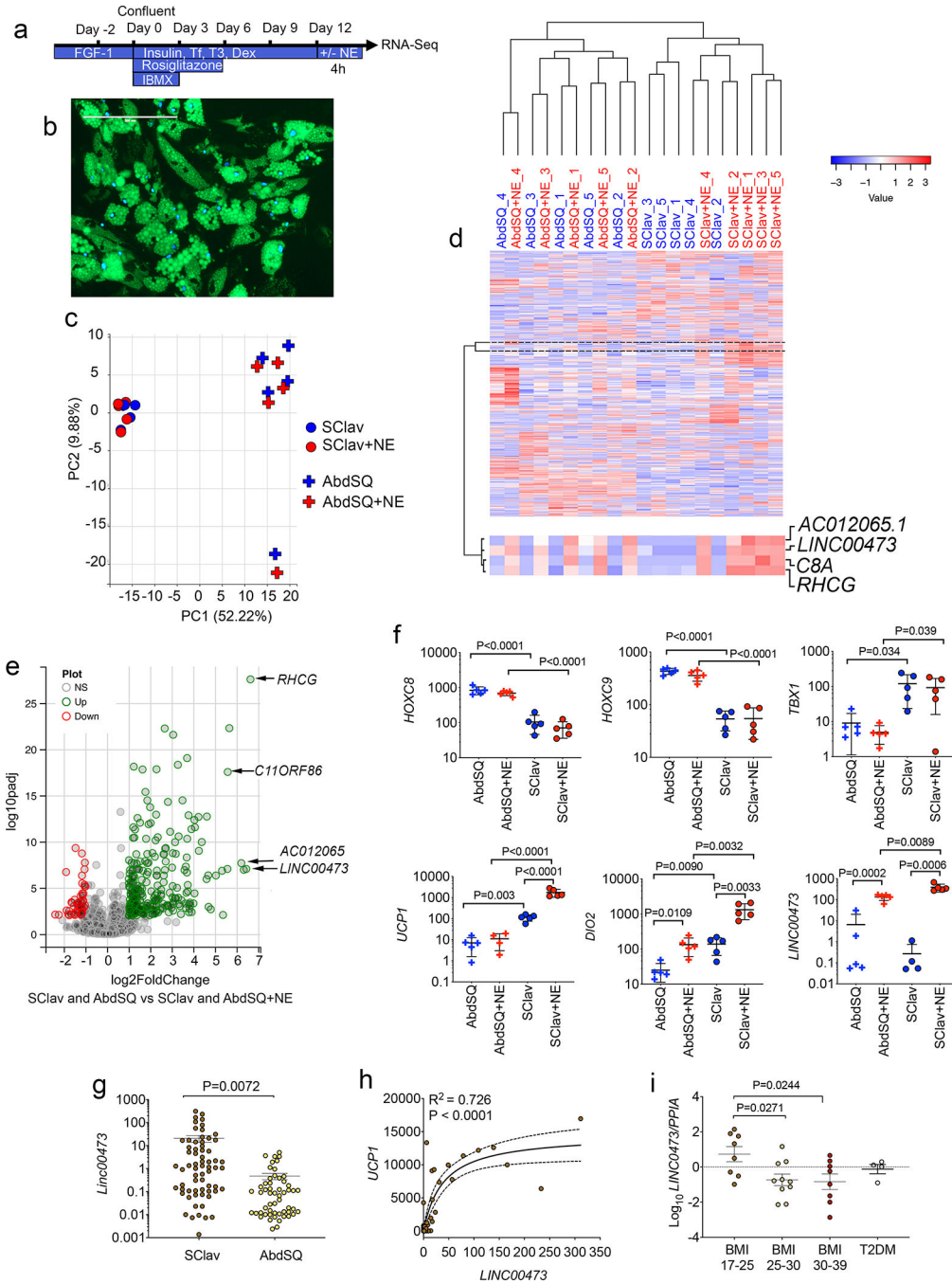


Figure 1. Comparison of gene expression in primary adipocytes from thermogenic and non-thermogenic human adipose tissue.
a. Scheme for differentiation of primary adipocytes from stromovascular fraction. **b.** Example of differentiated adipocytes from abdominal subcutaneous (AbdSQ) depot, showing lipid droplets marked by Bodipy (green), and nuclei labeled with Dapi (blue). Scale bar=200µm. This experiment was repeated 3 times with similar results. **c.** Principal component analysis of the 1000 most differentially expressed genes between primary adipocytes from supraclavicular (SCLav) or AbdSQ adipose tissue, without or with treatment

with norepinephrine (NE), derived from RNASeq of samples from n=5 independent subjects. **d.** Unsupervised hierarchical clustering using Pearson's correlation of same gene set used in panel (c). Marked is a cluster of genes exhibiting increased expression in response to NE in all depots. **e.** Volcano plot of genes differentially expressed in primary adipocytes in response to norepinephrine (NE) treatment. DESeq of datasets derived from adipocytes from 2 depots (SCLav and AbdSQ) from 5 independent subjects, n=10 datasets without NE and n=10 datasets with NE. **f.** FPKM values for selected genes. Plotted are individual values, means and SEM for n=5 cell lines derived from 5 independent subjects. Statistical differences between selected pairs (AbdSQ vs. AbdSQ+NE; AbdSQ vs. SCLav; SCLav vs. SCLav+NE; AbdSQ+NE vs SCLav+NE) were calculated using up-paired, two-tailed student t-tests, and where P values are < 0.05, exact P values are shown. **g.** Levels of *LINC00473* in adipose tissue sampled from SCLav or AbdSQ regions. Plotted are individual FPKM values, means and SEM of n=66 independent samples from separate individuals. Statistical significance of the difference was calculated using un-paired, two-tailed student t-test. **h.** Correlation between *UCP1* and *LINC00473* values in the cohort (n=66). Data were fitted using least squares regression without weighing or special handling of outliers as implemented by Prism 8. Exact P and R² values are shown. **i.** RT-PCR of *LINC00473* in tissue sampled from SCLav adipose tissue from individuals with the conditions depicted in the x-axis. Values are the expression of *LINC00473* relative to PPIA used as a housekeeping control. Plotted are individual values, means and SEM of n=8 (BMI 17–25), n=10 (BMI 25–30), n=8 (BMI 30–39), and n=4 (T2DM) samples from independent subjects. Statistical differences relative to BMI 17–25 were calculated using one-way ANOVA, with Dunnett's correction for multiple comparisons. Exact P values are shown.

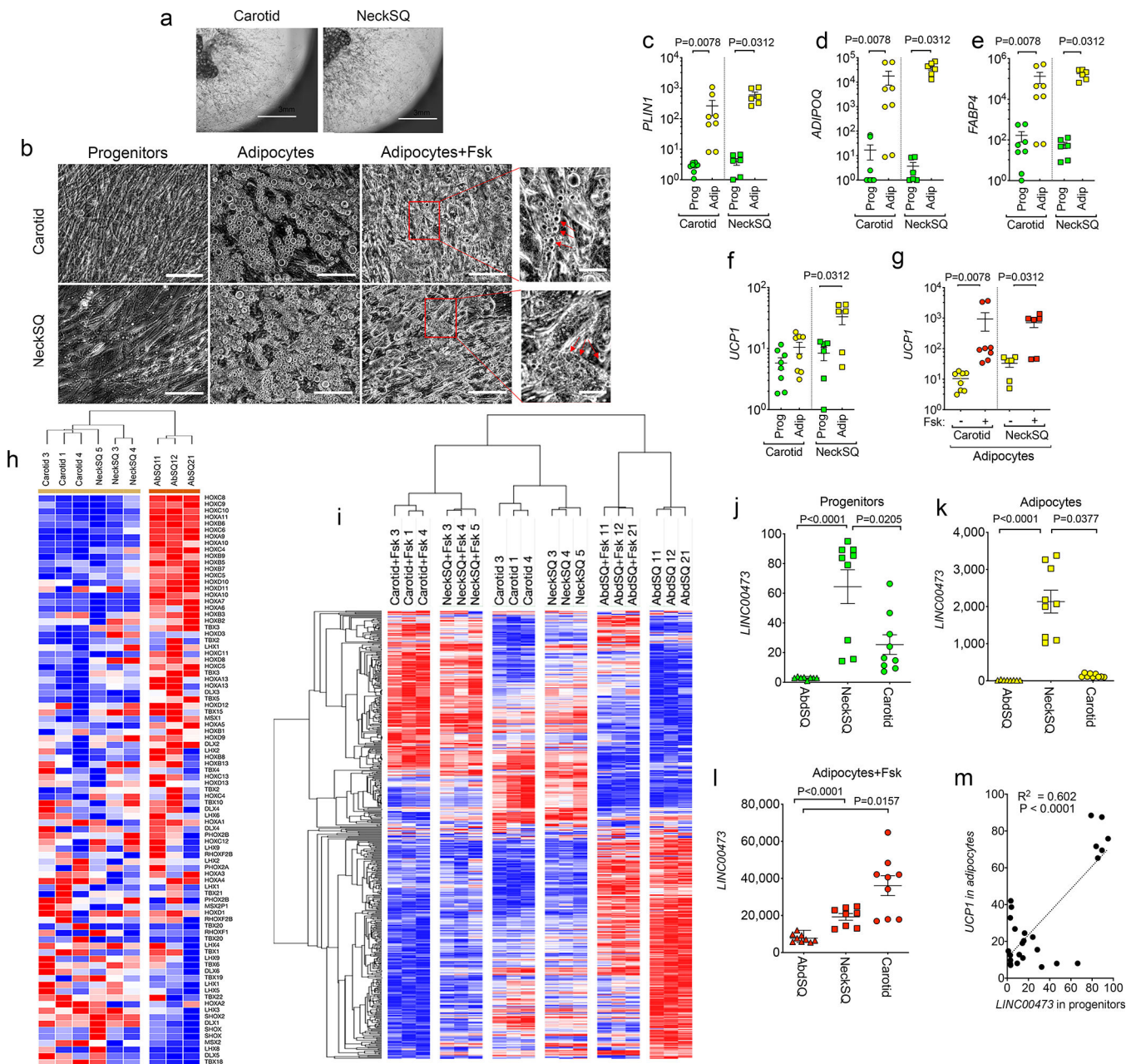


Figure 2. *LINC00473* expression is associated with thermogenic adipocyte development.
a. Example of explants from the indicated depots embedded in Matrigel and cultured for 10 days, showing sprouting and proliferation of progenitors. Similar results were seen in n=10 explants from samples from 3 independent individuals. **b.** Progenitors from Carotid or NeckSQ depots plated on plastic, after differentiation with adipogenic media (adipocytes), and after differentiation and exposure to Fsk daily for the last 5 days in culture (adipocytes +Fsk). Arrowheads in expanded images point to small lipid droplets in cells after Fsk stimulation. Similar results were seen in n=3 cultures from samples from 3 independent individuals. Scale bars=200 μ m. **c-f.** RT-PCR for the genes indicated on the y-axes, from progenitors (Prog) or differentiated adipocytes (Adip) derived from the Carotid or NeckSQ

depots as indicated on the x-axis. Values represent the fold-difference over the lowest detected value. Shown are individual values, mean and SEM for n=8 (Carotid progenitors and adipocytes) and n=6 (NeckSQ progenitors and adipocytes) values obtained from 2 independent cultures of cells derived from 3 or 4 different individuals (NeckSQ or Carotid, respectively). **g.** RT-PCR for *UCPI* in adipocytes from Carotid or NeckSQ with or without Fsk stimulation as indicated in the x-axes. Shown are individual values, mean and SEM of n=8 (Carotid adipocytes) and n=6 (NeckSQ adipocytes) biologically independent samples, as described above. For c-g, statistical significance of the differences was calculated using one-way ANOVA corrected for multiple comparisons using the Holm-Sidak method. **h.** Hierarchical clustering of mean probe intensity values for developmental genes in adipocytes derived from Carotid, NeckSQ and AbdSQ depots from three separate individuals. **i.** Unsupervised hierarchical clustering of genes showing the largest coefficient of variation (range 0.1 to 0.4) in control and Fsk-treated adipocytes derived from Carotid, NeckSQ and AbdSQ depots from three individuals. **j-l.** RT-PCR of *LINC00473* mRNA in cells derived from the depot indicated in the x-axis. Shown are individual values, means and SEM of n=9 biologically independent cultures derived from 3 different subjects. Statistical differences were calculated using the Krustal-Wallis test for non-parametric distributions, corrected for multiple comparisons using the Dunn's test. The exact P values are shown. **m.** Simple linear regression analysis between *LINC00473* values in progenitors and *UCPI* expression in corresponding adipocytes from cultures from Carotid, NeckSQ and AbdSQ depots, representing n=26 biologically independent samples.

incubated with extracts from Fsk-treated or non-treated cells (-Fsk or +Fsk), hybridized with or without *LINC00473*-specific biotinylated probes. Shown are LFQ values for the top 50 proteins ranked by the ratio of (+Fsk/-Fsk with specific probes)/(+Fsk/-Fsk without specific probes). Similar results were seen in three independent experiments **g**. Pathway analysis for GO cellular compartment of proteins identified in (f), as implemented by Kaimal et al ⁴⁹. **h**. RT-PCR values for *LINC00473* in control or PLIN1 immunoprecipitants of crosslinked extracts from non-treated or norepinephrine-treated adipocytes. Values are mean and SEM for n=4 biological replicates assayed with no technical replication **i**. Representative western blot of immune precipitates from three separate cultures of norepinephrine-treated adipocytes used for RT-PCR in panel (h), probed with antibody to PLIN1.

Author Manuscript

Author Manuscript

Author Manuscript

Author Manuscript

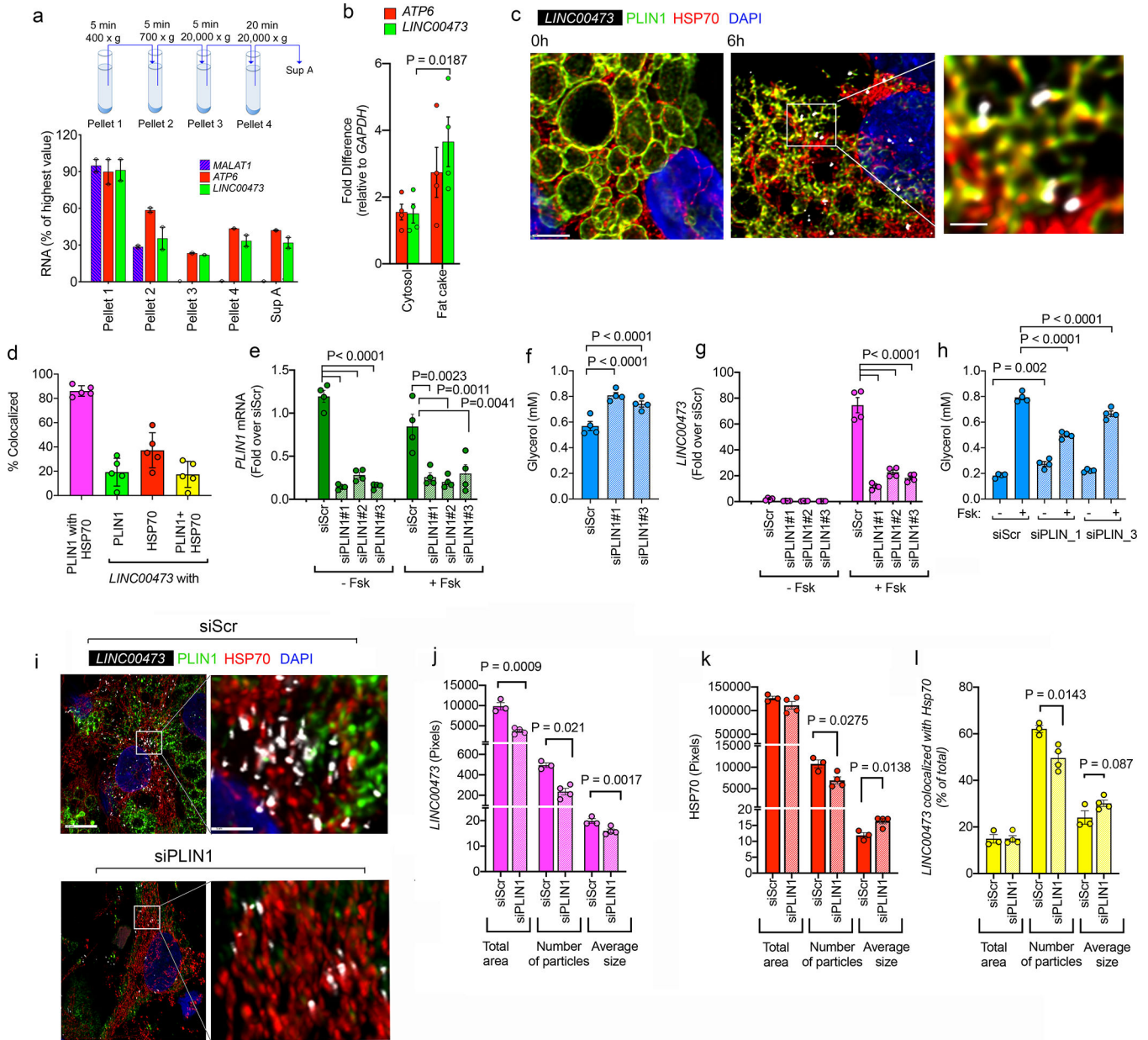


Figure 4.
a Schematic illustration of fractionation protocol, and RT-PCR for *MALAT1*, *ATP6* and *LINC00473* in subcellular fractions of adipocytes collected after stimulation with 10 μ M Fsk for 6 h. Shown are means and ranges for n=2 independent experiments. **b.** RT-PCR for *ATP6* and *LINC00473* in the cytosolic and floating fat fractions. Shown are each value for n=3 independent experiments, and bars represent the means and error lines the SEM. Statistical significance of the difference was calculated using paired, two-tailed student t-tests. **c.** Maximal intensity projections of confocal stacks of adipocytes stained with antibodies to mitochondrial HSP70 (red) and PLIN1 (green) following in-situ hybridization of *LINC00473* (white) in adipocytes stimulated with 10 μ M Fsk for 6 h. Scale bars = 5 μ m and

1 μm in expanded region. This image is representative of a minimum of 10 independent images from 4 samples prepared from cells from 2 different subjects. **d.** Extent of co-localization between HSP70, PLIN1 and *LINC00473* in adipocytes stimulated with 10 μM Fsk for 6h. Shown are individual values, means and SEM from n=5 independent images. **e.** RT-PCR of *PLIN1* 48h after transfection of adipocytes with scrambled (siScr) and three different PLIN1-directed siRNA oligonucleotides (siPLIN1#1–3) and stimulation for 6h with vehicle or 10 μM Fsk. Values are the means and SEM of n=4 independent experiments. **f.** Glycerol accumulation during 48h after transfection of cells as described in panel (e). Values are the means and SEM of n=4 biological replicates. **g.** RT-PCR of *LINC00473* 48h after transfection of adipocytes with scrambled (siScr) and three different PLIN1-directed siRNA oligonucleotides (siPLIN1#1–3) and stimulation for 6h with vehicle or 10 μM Fsk. Values are the means and SEM of n=4 independent experiments. **h.** Glycerol accumulation in the media during 6h of vehicle or Fsk treatment of cells transfected as described in panel (g). Values are the means and SEM from two independent experiments performed in duplicate wells with no technical replication for glycerol measurement n=4. This experiment has been replicated with cells from a different donor, with similar results. For **e, f, g, and h**, statistical significance of the differences was estimated using ordinary one-way ANOVA corrected for multiple comparisons using the Holm-Sidak test. **i.** Maximal intensity projections of confocal stacks of cells stained with antibodies to mitochondrial HSP70 (red) and PLIN1 (green) following in-situ hybridization of *LINC00473* (white) in adipocytes transfected with scrambled (siScr) or PLIN1-directed siRNA oligonucleotide (siPLIN1#1), stimulated with 10 μM Fsk for 6h, 48h following transfection. **j-l.** Image analysis of *LINC00473* (j) HSP70 (k), and of areas of *LINC00473* and HSP70 co-localization (l). Bars are means and error lines the SEM of n=4 independent fields each for siScr and SiPLIN1, each containing an average of 10 cells. Statistical significance of the differences between Scr and siPLIN1 for each molecule and for each parameter was calculated using un-paired, two-tailed student t-tests.

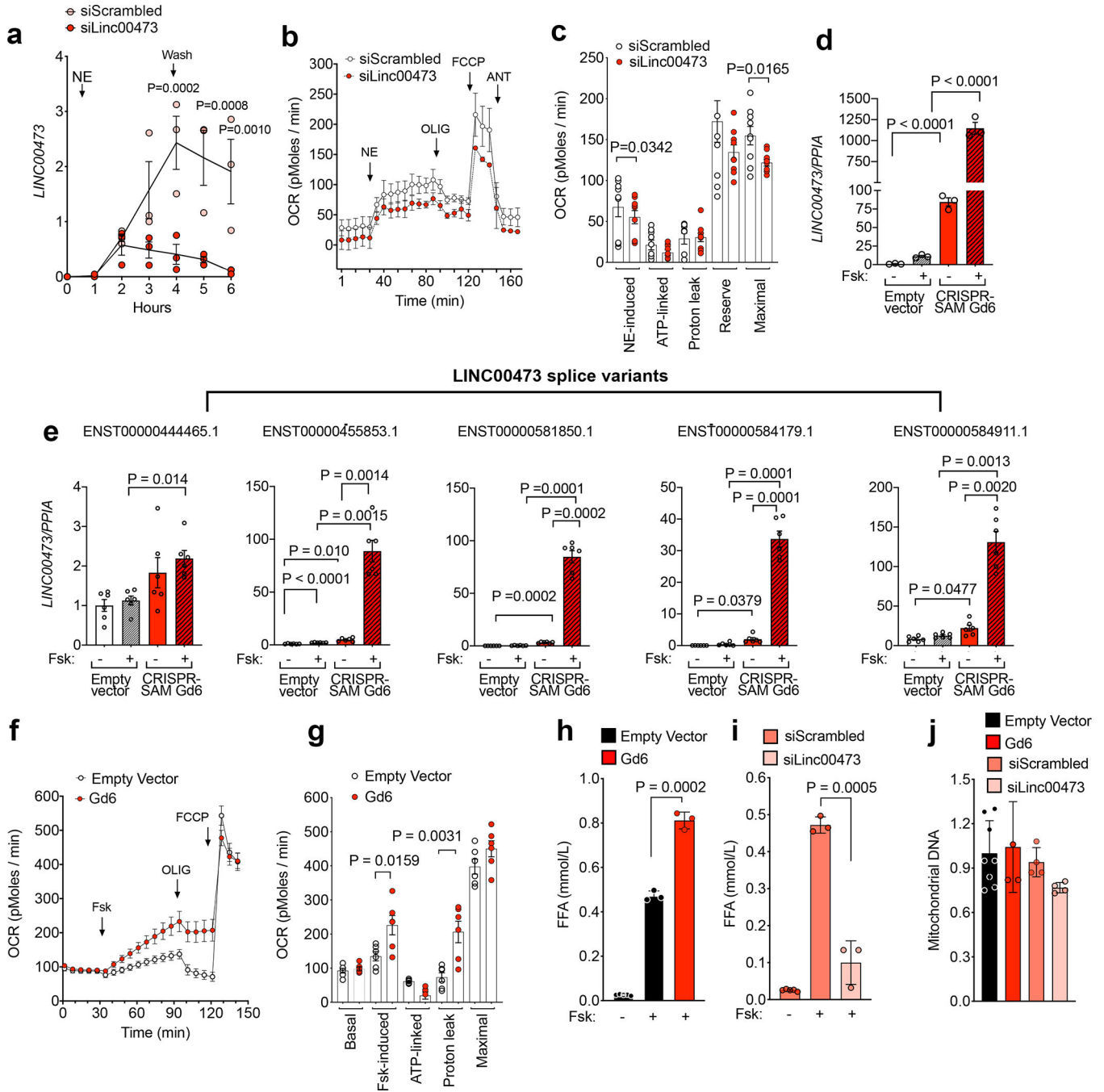


Figure 5. Functional role of *LINC00473*.

a. RT-PCR of *LINC00473* in SC1av treated with control or *LINC00473*-directed siRNA oligos 48h prior to stimulation with NE. Plotted are individual values, means and SEM at each time point of n=3 independent experiments. Statistical differences relative to control (siScrambled) were calculate using ANOVA corrected for multiple comparisons using the Holm-Sidak test. **b.** Oxygen consumption in primary adipocytes at day 12 of differentiation, treated with scrambled or *LINC00473* targeted siRNAs 72 h prior to assay. Indicated are the times of addition of norepinephrine (NE), Oligomycin (OLIG), FCCP, and rotenone/

antimycin (ANT) at concentrations indicated in Methods. Values are means and SEM of three experiments (n=3). **c.** Mitochondrial respiratory parameters were calculated using three paired time points per condition, per experiment, for an n=9 as follows: NE-induced=NE minus Basal; ATP-linked=NE minus OLIG; Proton leak=ANT minus OLIG; Respiratory reserve capacity=FCCP minus Basal; Maximal Respiratory Capacity=FCCP minus ANT. Plotted are the individual values, means and SEM. Statistical significance between Control and si*LINC00473* were calculated using paired, 2-tailed student t-tests. **d,e.** Expression levels of the major isoform of *LINC00473* (d) and of 5 splice variants (e) in adipocytes expressing either empty vector or overexpressing *LINC00473* through the CRISPR-SAM guide 6 (Gd6), stimulated with 10 μ M Fsk for 6 hours. Shown are the individual values, means and SEM of data from n=6 independent cell cultures. Statistical significance of differences was calculated using ANOVA corrected for multiple comparisons using the Sidak test. **f,g.** Oxygen consumption rates (f), and respiratory parameters (g) in adipocytes expressing either empty vector or Gd6. Indicated are the times of addition of Forskolin (Fsk), Oligomycin (OLIG), and FCCP. Plotted in (f) are the means and SEM of six experiments performed in triplicate using two cell populations (n=6). Plotted in (g) are the means and SEM of the respiratory parameters calculated for each experiment (n=6). Statistical significance between Empty Vector and Gd6 and si*LINC00473* were calculated using paired, 2-tailed student t-tests. **h,i.** Free fatty acids (FFA) (mmol/L) in media with and without Fsk stimulation in adipocytes expressing either empty vector or Gd6, (h) and in Gd6 cells transfected with scrambled (siScrambled) or *LINC00473*-directed (si*LINC00473*) pools of siRNA oligonucleotides (i). Plotted are the individual values, means and SEM of n=3 (FSK stimulation), and n=5 (without stimulation) independent cell cultures. **j.** Mitochondria DNA levels in cells treated as in panels h,i. Plotted are the individual values, means and SEM of n=8 (Empty Vector) and n=4 (Gd6, siScrambled and si*LINC00473*) independent cell cultures.

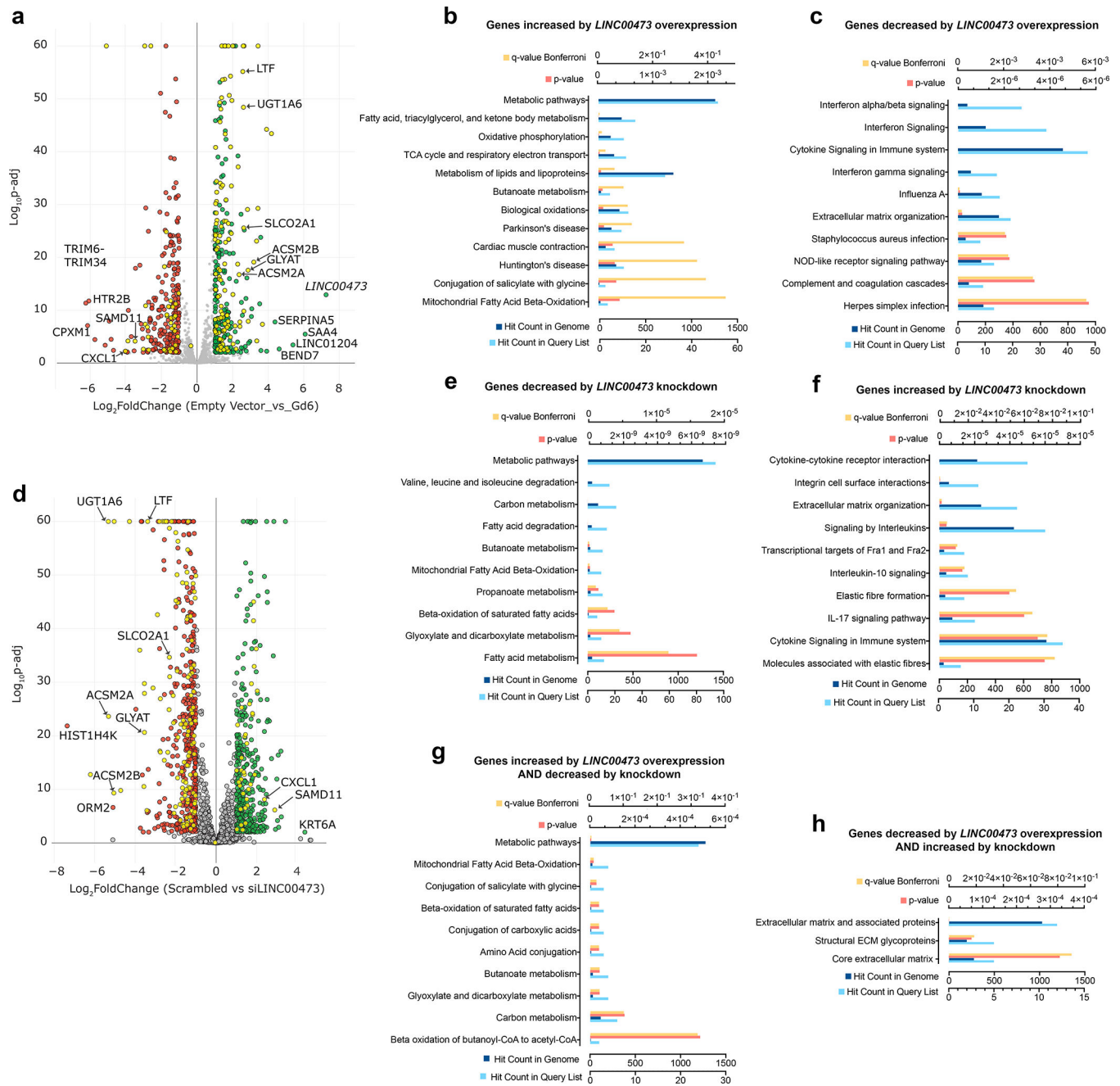


Figure 6. Transcriptomic changes in response to modulation of *LINC00473*.

a. Volcano plot of genes differentially expressed in cells overexpressing *LINC00473* through the CRISPR-SAM guide 6 (Gd6). RNASeq data obtained from n=4 (empty vector) and n=3 (Gd6) independent cell cultures was compared. **b.** Pathways enriched in genes that were increased in Gd6 cells compared to empty vector. **c.** Pathways enriched in genes that were decreased in Gd6 cells compared to empty vector. **d.** Volcano plot of genes differentially expressed in Gd6 cells transfected with scrambled compared to directed (siLINC00473) pools of siRNA oligonucleotides. RNASeq data obtained from n=4 (Scrambled) and n=4 (siLINC00473) independent cell cultures was compared. **e.** Pathways enriched in genes that

were decreased by *LINC00473* siRNA. **f.** Pathways enriched in genes that were increased by *LINC00473* siRNA. Yellow symbols in (a) and (d) depict genes that were reciprocally regulated by overexpression and depletion of *LINC00473*. **g.** Pathways enriched in genes that were increased in cells overexpressing *LINC00473* AND decreased in cells where *LINC00473* was knocked down. **h.** Pathways enriched in genes that were decreased in cells where *LINC00473* was overexpressed AND decreased in cells where *LINC00473* was knocked down.

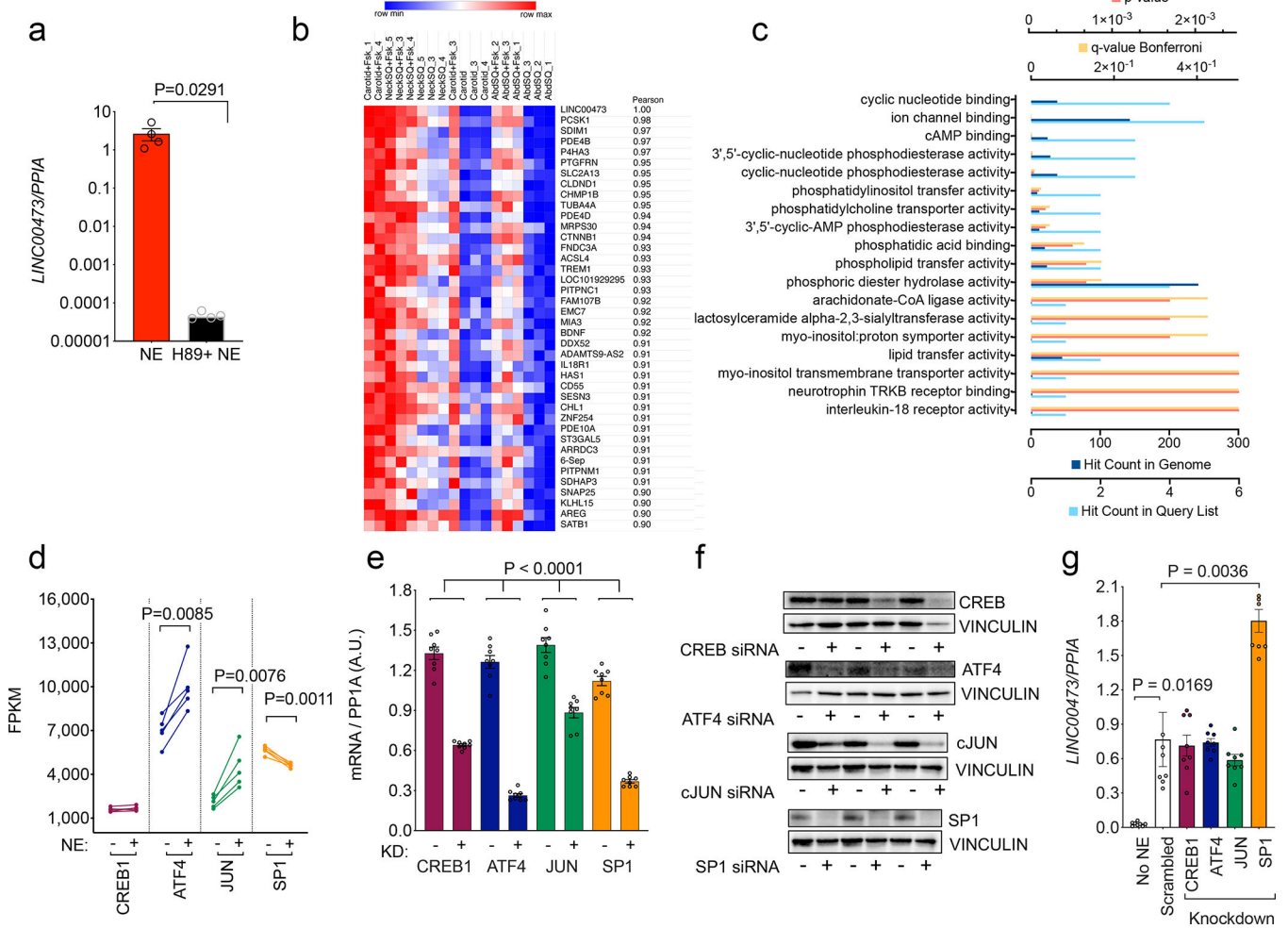


Figure 7. Mechanisms of induction of *LINC00473*.
a. *LINC00473* levels in NE-stimulated primary adipocytes from SClav exposed to vehicle or the adenylyl cyclase inhibitor H89 prior to stimulation. Shown are individual values, means and SEM of n=4 experiments. Statistical significance of the difference was calculated using unpaired, two-tailed student t-test. **b.** Heatmap of genes correlated with *LINC00473* with a spearman correlation coefficient of 0.9 or greater across cells from 3 different depots from 3 different subjects under two treatment conditions (- and +Fsk) as described in Figure 2. **c.** Pathway enrichment analysis of genes in (b). **d.** Expression levels of transcription factors predicted to regulate *LINC00473* expression. Plotted in before-after format are individual values from cells from 5 different subjects treated without (-) or with (+) NE. Statistical significance of the differences was calculated using paired, two-tailed student t-tests. **e.** Knockdown efficiency of indicated transcription factors. Plotted are the individual values, means and SEM of values from n=8 independent experiments. Statistical significance of the differences was calculated using paired, two-tailed student t-tests. **f.** Western blots of the transcription factors targeted by siRNA as in (e) using extracts from n=3 independent cell cultures. **g.** Expression levels of *LINC00473* in cells where the indicated transcription factors were knocked down, as in panel (e). Plotted are individual values, means and SEM of

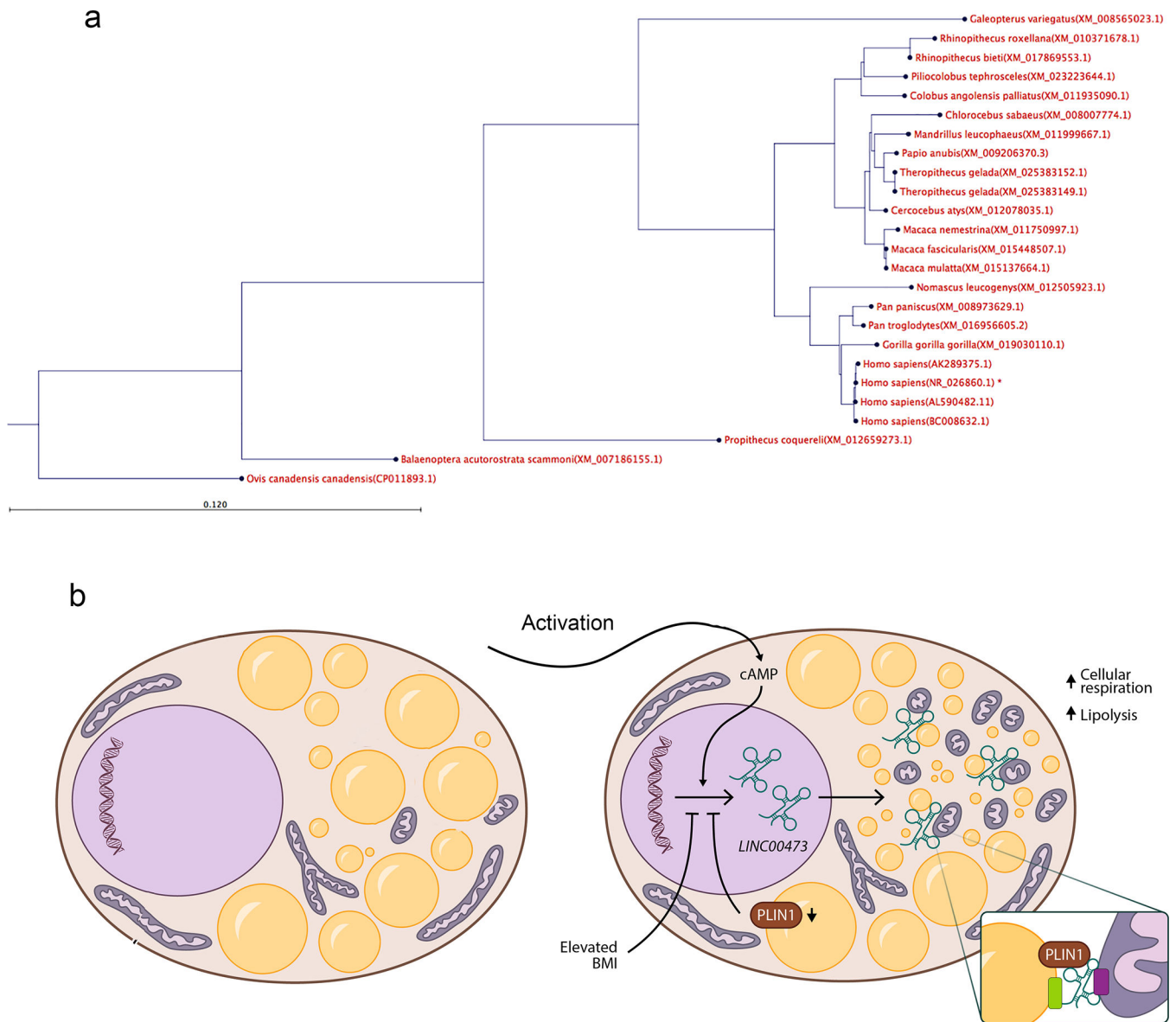
n=8 independent experiments. Statistical significance of differences was calculated using one-way ANOVA corrected for multiple comparisons using the Holm-Sidak method.

Author Manuscript

Author Manuscript

Author Manuscript

Author Manuscript



Human Thermogenic Adipocytes

Figure 8: Phylogenetic analysis and conceptual function model for *LINC00473*.

a. We used BLASTN 2.8.0+ against “nr” database to find orthologs of the NR_026860.1 (Homo sapiens long intergenic non-protein coding RNA 473 (*LINC00473*), transcript variant 1, long non-coding RNA molecule type nucleic acid) in other organisms. To be as inclusive as possible we used the “More dissimilar sequences” (discontiguous megablast) option. We detected 243 homolog sequences from the blast. The pairwise sequence distances were used to generate a phylogenetic tree using fast minimum evolution tree method with 0.65 cut-off for maximum sequence differences. Although we did find some homolog sequences in primates, we did not detect any significant homolog sequence in lower eukaryotes. **b.** Conceptual model in which *LINC00473* expression regulates inter-organelle communication upon activation. Activation of thermogenic adipocytes leads to cAMP-

dependent expression and cytoplasmic translocation of *LINC00473* to the lipid droplet-mitochondria interface, where it forms multimeric complexes that include PLIN1. Through these interactions, lipolysis and mitochondrial respiration are activated. A feedback loop where PLIN1 levels influence *LINC00473* expression contributes to this regulatory mechanism.

Author Manuscript

Author Manuscript

Author Manuscript

Author Manuscript